



TEZ ŞABLONU ONAY FORMU
THESIS TEMPLATE CONFIRMATION FORM

1. Şablonda verilen yerleşim ve boşluklar değiştirilmemelidir.
2. **Jüri tarihi** Başlık Sayfası, İmza Sayfası, Abstract ve Öz'de ilgili yerlere yazılmalıdır.
3. İmza sayfasında jüri üyelerinin unvanları doğru olarak yazılmalıdır. Tüm imzalar **mavi pilot kalemle** atılmalıdır.
4. **Disiplinlerarası** programlarda görevlendirilen öğretim üyeleri için jüri üyeleri kısmında tam zamanlı olarak çalıştıkları anabilim dalı başkanlığının ismi yazılmalıdır. Örneğin: bir öğretim üyesi Biyoteknoloji programında görev yapıyor ve biyoloji bölümünde tam zamanlı çalışıyorsa, İmza sayfasına biyoloji bölümü yazılmalıdır. İstisnai olarak, disiplinler arası program başkanı ve tez danışmanı için disiplinlerarası program adı yazılmalıdır.
5. Tezin **son sayfasının sayfa** numarası Abstract ve Öz'de ilgili yerlere yazılmalıdır.
6. Bütün chapterlar, referanslar, ekler ve CV sağ sayfada başlamalıdır. Bunun için **kesmeler** kullanılmıştır. **Kesmelerin kayması** fazladan boş sayfaların oluşmasına sebep olabilir. Bu gibi durumlarda paragraf (¶) işaretine tıklayarak kesmeleri görünür hale getirin ve yerlerini **kontrol edin**.
7. Figürler ve tablolar kenar boşluklarına taşmamalıdır.
8. Şablonda yorum olarak eklenen uyarılar dikkatle okunmalı ve uygulanmalıdır.
9. Tez yazdırılmadan önce PDF olarak kaydedilmelidir. Şablonda yorum olarak eklenen uyarılar PDF dokümanında yer almamalıdır.
10. **Bu form aracılığıyla oluşturulan PDF dosyası arkalı-önlü baskı alınarak tek bir spiralli cilt haline getirilmelidir.**
11. Spiralli hale getirilen tez taslağınızdaki ilgili alanları imzalandıktan sonra, [Tez Jüri Atama Formu](#) ile birlikte bölüm sekreterliğine teslim edilmelidir.
12. Tez taslaklarının kontrol işlemleri tamamlandığında, bu durum öğrencilere METU uzantılı öğrenci e-posta adresleri aracılığıyla duyurulacaktır.
13. Tez yazım süreci ile ilgili herhangi bir sıkıntı yaşarsanız, [Sıkça Sorulan Sorular \(SSS\)](#) sayfamızı ziyaret ederek yaşadığınız sıkıntıyla ilgili bir çözüm bulabilirsiniz.
1. Do not change the spacing and placement in the template.
2. Write **defense date** to the related places given on Title page, Approval page, Abstract and Öz.
3. Write the titles of the examining committee members correctly on Approval Page. **Blue ink** must be used for all signatures.
4. For faculty members working in **interdisciplinary programs**, the name of the department that they work full-time should be written on the Approval page. For example, if a faculty member staffs in the biotechnology program and works full-time in the biology department, the department of biology should be written on the approval page. Exceptionally, for the interdisciplinary program chair and your thesis supervisor, the interdisciplinary program name should be written.
5. Write **the page number of the last page** in the related places given on Abstract and Öz pages.
6. All chapters, references, appendices and CV must be started on the right page. **Section Breaks** were used for this. **Change in the placement** of section breaks can result in extra blank pages. In such cases, make the section breaks visible by clicking paragraph (¶) mark and **check their position**.
7. All figures and tables must be given inside the page. Nothing must appear in the margins.
8. All the warnings given on the comments section through the thesis template must be read and applied.
9. Save your thesis as pdf and Disable all the comments before taking the printout.
10. **Print two-sided the PDF file that you have created through this form and make a single spiral bound.**
11. Once you have signed the relevant fields in your thesis draft that you spiraled, submit it to the department secretary together with your [Thesis Jury Assignment Form](#).
12. This will be announced to the students via their METU students e-mail addresses when the control of the thesis drafts has been completed.
13. If you have any problems with the thesis writing process, you may visit our [Frequently Asked Questions \(FAQ\)](#) page and find a solution to your problem.

Yukarıda bulunan tüm maddeleri okudum, anladım ve kabul ediyorum. / I have read, understand and accept all of the items above.

Name : İsmail Harun
Surname : Hökelek
E-Mail : harun.hokelek@metu.edu.tr
Date : 07.02.2022
Signature : _____

OPTIMUM PLACEMENT AND COST-BENEFIT ANALYSIS OF
BATTERY ENERGY STORAGE SYSTEMS

A THESIS SUBMITTED TO
THE GRADUATE SCHOOL OF NATURAL AND APPLIED SCIENCES
OF
MIDDLE EAST TECHNICAL UNIVERSITY

BY

İSMAİL HARUN HÖKELEK

IN PARTIAL FULFILLMENT OF THE REQUIREMENTS
FOR
THE DEGREE OF MASTER OF SCIENCE
IN
ELECTRICAL AND ELECTRONICS ENGINEERING

FEBRUARY 2022

Approval of the thesis:

**OPTIMUM PLACEMENT AND COST-BENEFIT ANALYSIS OF
BATTERY ENERGY STORAGE SYSTEMS**

submitted by **İSMAİL HARUN HÖKELEK** in partial fulfillment of the requirements for the degree of **Master of Science in Electrical and Electronics Engineering, Middle East Technical University** by,

Prof. Dr. Halil Kalıpçılar
Dean, Graduate School of **Natural and Applied Sciences**

Prof. Dr. İlkay Ulusoy
Head of the Department, **Electrical and Electronics Eng.**

Prof. Dr. Ali Nezh Güven
Supervisor, **Electrical and Electronics Eng., METU**

Examining Committee Members:

Assoc. Prof. Dr. Murat Göl
Electrical and Electronics Eng., METU

Prof. Dr. Ali Nezh Güven
Electrical and Electronics Eng., METU

Prof. Dr. Saffet Ayasun
Electrical and Electronics Eng., Gazi Uni.

Prof. Dr. Müslüm Cengiz Taplamacıoğlu
Electrical and Electronics Eng., Gazi Uni.

Assoc. Prof. Dr. Ozan Keysan
Electrical and Electronics Eng., METU

Date: 07.02.2022

I hereby declare that all information in this document has been obtained and presented in accordance with academic rules and ethical conduct. I also declare that, as required by these rules and conduct, I have fully cited and referenced all material and results that are not original to this work.

Name Last name: İsmail Harun Hökelek

Signature:

ABSTRACT

OPTIMUM PLACEMENT AND COST-BENEFIT ANALYSIS OF BATTERY ENERGY STORAGE SYSTEMS

Hökelek, İsmail Harun
Master of Science, Electrical and Electronics Engineering
Supervisor: Prof. Dr. Ali Nezih Güven

February 2022, 97 pages

There are many challenges associated with the integration of Battery Energy Storage Systems (BESS) into the power system. Some of these challenges are determining the sizing of BESS and finding the optimum placement of these devices in the grid. The primary motivation of this study is to handle the placement and sizing problem of BESS.

In the vast majority of studies, the optimum BESS locations have been found by calculating loss sensitivity factor (LSF) under peak load conditions. However, this approach will not give the optimum location of storage devices since it does not cover both the charging and discharging operation modes of BESS. To overcome this problem, a revised approach that considers both operation modes of battery has been performed, and this method is referred to as Δ LSF in this thesis. The Δ LSF method was implemented on three test systems, and the results were verified by load flow analysis.

In addition, a cost-benefit analysis method has been applied to find the capacity and power ratings of BESS. In this study, placement and sizing methods are based on storing energy when the electricity market price is low and returning the stored energy to the grid during peak price hours to obtain financial savings. Grid losses

reduction due to BESS operation has also been considered in savings. In the cost-benefit analysis, numerical calculation results were given to verify that the financial savings cover the investment cost of the battery. Simulations and analysis calculations have been implemented on MATLAB environment.

Keywords: Battery Energy Storage Systems, Loss Sensitivity Factor, Optimum BESS Placement, Energy Trading, BESS Capacity Sizing

ÖZ

BATARYA ENERJİ DEPOLAMA SİSTEMLERİNİN OPTİMUM KONUMLANDIRILMASI VE MALİYET-FAYDA ANALİZİ

Hökelek, İsmail Harun
Yüksek Lisans, Elektrik ve Elektronik Mühendisliği
Tez Yöneticisi: Prof. Dr. Ali Nezih Güven

Şubat 2022, 97 sayfa

Batarya Enerji Depolama Sistemlerinin (BESS) güç sistemine entegrasyonu ile ilgili birçok zorlukla karşılaşmaktadır. Güç sisteminde optimum batarya konumlandırılmasını bulmak ve batarya kapasitesini belirlemek bu zorluklardan bazılarıdır. Bu çalışmanın temel motivasyonu, BESS'lerin konumlandırılma ve kapasite boyutlandırma problemlerini ele almaktır.

Önceki çalışmaların birçoğunda, maksimum yük koşullarındaki kayıp hassasiyet faktörü (LSF) hesaplanarak BESS konumları bulunmuştur. Ancak bu yaklaşım, BESS'lerin hem şarj hem de deşarj çalışma modlarını kapsamadığı için bataryanın optimum konumlandırmasını vermeyecektir. Bahsedilen problemin üstesinden gelebilmek için, bataryanın her iki çalışma modunu kapsayan revize edilmiş bir yaklaşım uygulanmış, ve tez içerisinde bu metod Δ LSF olarak adlandırılmıştır. Δ LSF metodu üç test sistemi üzerinde denenmiş, ve sonuçlar güç akış analizi yapılarak doğrulanmıştır.

Buna ek olarak, BESS kapasite ve güç değerlerini bulmak için maliyet-fayda analizine dayalı bir yöntem uygulanmaktadır. Bu tezde, optimum bara lokasyonu bulma ve kapasite belirleme metodlarında, elektrik piyasa fiyatlarının düşük olduğu

zamanlarda enerjinin depolanması ve en yüksek piyasa fiyatının olduğu zamanlarda depolanan enerjinin şebekeye geri verilmesi ile finansal fayda sağlanması durumu incelenmektedir. BESS'in çalışmasından dolayı sistem kayıplarında oluşan azalma da finansal getiri hesaplanırken dikkate alınmıştır. Maliyet-fayda analizinde, elde edilen finansal getirilerin batarya yatırım maliyetini karşıladığını doğrulamak için nümerik hesaplamalar yapılmıştır. Simülasyon ve analiz hesaplamalarında MATLAB kullanılmıştır.

Anahtar Kelimeler: Batarya Enerji Depolama Sistemleri, Kayıp Hassasiyet Faktörü, Optimum BESS Konumlandırma, BESS ile Elektrik Alım-Satımı, BESS Kapasite Hesaplama

To My Beloved Family

ACKNOWLEDGMENTS

Firstly, I would like to express my gratitude to my supervisor Prof. Dr. Ali Nezhil Güven, for his continuous guidance, encouragement, and support through all phases of this work. Apart from this thesis, he also led me throughout my journey at METU.

I would like to thank Göksel Sözeri for his recommendations and observations. All the time, he gave me opinions to overcome challenges.

I also have to thank my parents, Yılmaz Hökelek, Rüyeyda Hökelek, and Kübra Hökelek, for their endless support and belief. They have my utmost respect.

Finally, I am genuinely grateful to Dicle Türköne for giving me the motivation and courage to complete this work. I feel blessed to have such a great person.

TABLE OF CONTENTS

ABSTRACT.....	v
ÖZ.....	vii
ACKNOWLEDGMENTS	x
TABLE OF CONTENTS.....	xi
LIST OF TABLES	xiii
LIST OF FIGURES	xv
LIST OF ABBREVIATIONS	xvii
CHAPTERS	
1 INTRODUCTION	1
1.1 Literature Research	3
1.2 Thesis Outline	7
2 BACKGROUND REVIEW	9
2.1 Electrical Grid	9
2.2 Daily Load Curve and Load Shifting	11
2.3 Evolution Process of Batteries	13
2.4 Time of Use Pricing	15
2.5 Distributed Generation, Microgrids and Load Shedding	16
2.6 Application Benefits That Motivate the Usage of BESS	19
2.7 Network Matrices	21
2.8 Power Flow Analysis	24
2.9 Transmission Loss Calculation	33
3 PROBLEM FORMULATION AND METHODOLOGY.....	41

3.1	Optimum BESS Placement	41
3.2	Cost-Benefit Analysis for Determination of BESS Sizing	48
4	TESTS AND EVALUATIONS	55
4.1	Optimal Placement of BESSs	55
4.2	Evaluation of Cost-Benefit Analysis According to BESS Sizes	77
4.3	Discussion on Testing and Evaluation	83
5	CONCLUSION AND FUTURE WORKS.....	85
	REFERENCES	87
	APPENDICES	
A.	IEEE 14-Bus Test Case Data	93
B.	9-Bus Test System Data.....	95
C.	IEEE 33-Bus Test System Data	96

LIST OF TABLES

TABLES

Table 2.1. The Potential Types of Ancillary Services that Can be Used for BESS Applications [19]	21
Table 2.2. Partial Differentiation of Equation 2.48.....	36
Table 3.1. BESS Discharging Cycles and Corresponding Capacity Depths [20]...	51
Table 3.2. Cost Reduction Rate of Batteries [20]	51
Table 3.3. Typical Pricing of BESSs Projected to Year 2022 [19].....	52
Table 4.1. Grid Losses During Operation of BESS for Test System-I	71
Table 4.2. Grid Losses During Operation of BESS for Test System-II.....	72
Table 4.3 Grid Losses During Operation of BESS for Test System-III	73
Table 4.4. Loss Reduction Rates Corresponds to P^B for Test System-I	77
Table 4.5. Savings Obtained from Loss Reduction Cost During the BESS’s Life for Test System-I and Daily Energy Price Curve-I	78
Table 4.6. Total Savings Obtained from Energy Trading and Loss Reduction with Corresponding BESS Power Ratings for Daily Energy Price Curve-I	80
Table 4.7. BESS Investment and Operation Cost for Corresponding Power and Capacity Ratings for Daily Energy Price Curve-I	80
Table 4.8. Savings Obtained from Loss Reduction Cost During the BESS’s Life for Test System-I and Daily Energy Price Curve-II	82
Table 4.9. Total Savings Obtained from Energy Trading and Loss Reduction with Corresponding BESS Power Ratings for Daily Energy Price Curve-II.....	82
Table 4.10 BESS Investment Cost and Total Savings Obtained from BESS Operation for Daily Energy Price Curve-II.....	83
Table A.1. IEEE 14-Bus System Bus Data.....	93
Table A.2. IEEE 14-Bus System Generator Data	93
Table A.3. IEEE 14-Bus System Branch Data.....	94
Table B.4. 9-Bus System Bus Data.....	95

Table B.5. 9-Bus System Generator Data	95
Table B.6. 9-Bus System Branch Data	95
Table C.7. IEEE 33-Bus System Bus Data.....	96
Table C.8. IEEE 33-Bus System Generator Data.....	97
Table C.9. IEEE 33-Bus System Branch Data	97

LIST OF FIGURES

FIGURES

Figure 2.1. Basic Model of Electrical Grid [22]	10
Figure 2.2. Turkey's Daily Load Curve for the Date 29.07.2019, Source: Energy Exchange Istanbul [23]	12
Figure 2.3. A Sample Microgrid System that has an Energy Storage Unit [31].....	17
Figure 2.4. Basic Circuit Model of a Transformer [36]	22
Figure 2.5. Diagram of a Transformer that has an Off-Nominal Turns Ratio [36]	23
Figure 2.6. Circuit Model of a Transformer that has an Off-Nominal Turns Ratio [36].....	23
Figure 3.1. Intraday Market Energy Prices on 29.07.2019, Source: Energy Exchange Istanbul [23]	44
Figure 3.2. Charging and Discharging Periods on Intraday Market Energy Prices Curve.....	45
Figure 3.3. Combination of Daily Load and Daily Energy Price Curves	46
Figure 3.4. The Relationship Between BESS Capacity and Discharging Cycle [21]	50
Figure 4.1. IEEE 14-Bus Test Case Single Line Diagram [38]	56
Figure 4.2. 9-Bus Test Case Single Line Diagram [39].....	57
Figure 4.3. IEEE 33-Bus Test Case Single Line Diagram [40]	57
Figure 4.4. Daily Load Curve Based on Country Load of Turkey, Spring Minimum, Date: 23.03.2020-29.03.2020 [23]	58
Figure 4.5. Daily Load Curve Based on Country Load of Turkey, Summer Peak, Date: 06.07.2020-12.07.2020 [23]	59
Figure 4.6. Daily Load Curve Based on Country Load of Turkey, Winter, Date: 10.12.2020-16.12.2020 [23].....	59
Figure 4.7. Daily Load Curve Obtained by Averaging Three Seasonal Data.....	60

Figure 4.8. Intraday Country Electrical Energy Prices of Turkey, Spring Minimum, Date: 23.03.2020-29.03.2020 [23]	61
Figure 4.9. Intraday Country Electrical Energy Prices of Turkey, Summer Peak, Date: 06.07.2020-12.07.2020 [23]	61
Figure 4.10. Intraday Country Electrical Energy Prices of Turkey, Winter, Date: 10.12.2020-16.12.2020 [23]	62
Figure 4.11. Intraday Electrical Energy Prices of Turkey Obtained by Averaging Three Seasonal Data	63
Figure 4.12. 24-Hours Daily Load Curve Obtained by Averaging Weekly Data ...	63
Figure 4.13. 24-Hours Electrical Energy Prices Curve Obtained by Averaging Weekly Data	64
Figure 4.14. Combination of 24-Hours Electrical Energy Prices and Daily Load Curves	65
Figure 4.15. Daily LSF Calculation for 14-Bus Test Case.....	66
Figure 4.16. Δ LSF Calculation for 14-Bus Test Case	67
Figure 4.17. Daily LSF Calculation for 9-Bus Test Case.....	68
Figure 4.18. Δ LSF Calculation for 9-Bus Test Case	68
Figure 4.19. Δ LSF Calculation for 33-Bus Test Case	69
Figure 4.20. Conventional LSF Calculation for Test System-III	74
Figure 4.21. Variation of Losses with Increased Injection by Two Loss Calculation Methods at Bus-8.....	76
Figure 4.22. Variation of Losses with Increased Injection by Two Loss Calculation Methods at Bus-9.....	76
Figure 4.23. Electrical Energy Prices of Illinois Institute of Technology Microgrid	81

LIST OF ABBREVIATIONS

ABBREVIATIONS

AC	Alternative Current
BESS	Battery Energy Storage System
BOP	Balance of Plant Cost
CC	Construction Cost
DC	Direct Current
DER	Distributed Energy Resources
DOD	Depth of Discharge
DOE	United States Department of Energy
EC	Energy Capacity Cost
EAC	Energy Arbitrage Cost
EXIST	Energy Exchange Istanbul
FL	Floating Life of BESS
IEEE	The Institute of Electrical and Electronics Engineers
IOC	Investment and Operation Cost
ITL	Incremental Transmission Loss
LRC	Loss Reduction Cost
LSF	Loss Sensitivity Factor
MW	Mega-Watt
MWh	Mega-Watt-Hours

OMC	Operation and Maintenance Cost
PC	Power Conversion Cost
PCC	Point of Common Coupling
PV	Photo-Voltaic
RE	Round-Trip Efficiency of BESS
TDCD	Time Duration of Charge/Discharge

CHAPTER 1

INTRODUCTION

Energy storage has always been one of the most challenging issues in history. For this reason, energy storage technologies are extensively explored by the academic community. Batteries are one of the subjects that are under the spotlight in these studies. The use of batteries in power system applications as the form of energy storage systems has become a more popular research and application topic today, and this type of system is called Battery Energy Storage System (BESS). The reason of popularization is that batteries have profound application areas such as regulation and storage of renewable resource generation, supplemental reserve for isolated microgrids, frequency control by grid utilities, and demand response applications. In addition, increased usage of electric vehicles provide an opportunity to individuals about using as a supplemental reserve or selling stored excessive energy to the market for taking advantage of variations in energy prices which is called vehicle-to-grid.

Battery storage systems can act as a load in the electrical network, as well as support the generation. For this reason, several issues have emerged that should be considered in the use of battery storage systems at large power values. Some of these problems can be shown as finding the optimum placement of BESS in a grid and determining the procedure of the sizing of BESS. In this thesis, studies on these two important issues are presented, finding optimal location and sizing of battery energy storage system. It is observed that the vast majority of the studies about these two topics are focused on one of these problems. In this thesis work, solution methods for both problems are proposed.

To solve the BESS placement problem, a method based on loss sensitivity factor (LSF) is investigated, which is the widely preferred method for this topic by researchers. LSF method determines the relation between transmission losses and

variation in injected power at that bus. It is realized that the conventional LSF approach considers that the battery works only in discharge mode. The drawback of this method is eliminated by implementing a modified version of the LSF method, namely Δ LSF. The basis of the Δ LSF method is that calculating many numbers of LSFs, and substituting LSF values refers to charging hours from LSF values belonging to discharging hours. According to the methodology, the bus with the highest Δ LSF value shows the optimum BESS location considering grid losses.

Moreover, a cost-benefit analysis is presented to determine the sizing of BESS according to investment cost. The main objective of this analysis is to return the BESS investment and operation expenses from savings obtained by trading energy in a day and loss reduction cost. Several costing parameters are defined to assess the BESS investment related to battery capacity, power conversion units, constructional expenses, auxiliary connection costs, and operational expenditures. In the scope of this analysis, the only consideration is that getting financial savings from energy trading application of BESS. However, BESS usage helps to ensure the reliable and continuous operation of the grid. The cost of BESS investment reduces day by day since the research on battery technology is advanced immensely, and this reduction rate is considered in the cost-benefit analysis.

After describing the problem and formulation of this study, the solution method for optimum BESS placement and the proposed cost-benefit analysis are evaluated. Three different test systems are selected for testing network, IEEE 14-Bus, 9-Bus, and IEEE 33-Bus test cases. The validation of the optimum BESS placement method is implemented by comparing grid losses with or without BESS. In the validation section, the accuracy of the Δ LSF method is presented. Also, conventional LSF method is executed for the IEEE 33-Bus test case to exhibit the drawback of this method, and to emphasize the selection reason of Δ LSF method for optimum BESS placement. The proposed cost-benefit analysis is evaluated for three different BESS power ratings, and two different energy market. The reason for choosing two distinct energy markets is to emphasize the importance of different energy price levels in a day to achieve the objective of obtaining savings from energy trading.

1.1 Literature Research

Initially, research was conducted on how BESSs were integrated into the power system. The case where BESSs are used to regulate variable outputs of renewable energy sources is examined. In the literature, there are BESS applications with the storage system integrated into renewable resources generation unit and acting as a controller. There are instantaneous wind power input, load and generation at that hour as input to the system. BESS controller collects these inputs and undertakes the task of charging the battery if the wind power at that hour is more than the predicted, and supporting as generator the system with the battery if the actual wind power is less than the estimated wind power. However, this approach can only be applied to regulate the renewable energy resources output. In study [1], it can be aimed to reduce the total investment and operation cost by using the conservation of voltage method and BESS together. This approach becomes effective when the voltage profile is above 1.0 per unit on most buses. In other studies, an objective function is defined that contains two parts. The first part of this objective function takes the difference between bus voltages before and after the integration of BESS, and the following part represents the total active power losses of the system. Finally, these two parts are added together with weighting factors for each other to find the objective function. The resulting objective function is tried to be minimized with techniques such as particle swarm optimization, reducing variable trend search, and differential evolution [2], [3]. García-Muñoz and Francisco Díaz-Gonzalez investigate a method to find the optimum sizing of BESS in a power system that meets all demand from renewable generation units and BESSs. Multiperiod AC power flow calculation is done to minimize the investment and operational costs. As a result, bus locations to install the BESS and capacity sizing of the storage system are provided [4]. In another approach, Essayeh examines a system that has PV generation integrated with BESS. In this study, the problem formulation is based on minimizing the total cost of a microgrid. Both sizing of BESS and renewable generation are calculated based on this formulation. The proposed methodology

covers the unpredictable output of renewables. Simulations are performed using the historical data for one-year load demand [5]. Zarezadeh et al. are also worked on PV and energy storage systems. Uncontrollable parameters of renewables are produced by using a Point Estimation Method (PEM). An objective function is constructed to minimize expected daily operation costs. This function is solved with Mixed Integer Programming (MIP) model. In this work, feed-in tariff and time-of-use tariff models are used for electricity market pricing. Authors indicate that electricity price difference in a day has extreme importance for sizing BESS and PV systems. It is underlined that the sizing of BESS and PV systems is independent when the market price difference is low [6]. Another study examines a residential place that has a rooftop solar unit. Photovoltaic output power is simultaneously monitored during the day, and the energy is stored when the photovoltaic output becomes more than the load. A cost function is introduced that includes PV-BESS investment costs, operating and maintenance costs considering the life cycle of both systems. The proposed method is used to find out the optimum sizing of the solar unit and BESS. It is stated PV-BESS integration will be a significantly economical choice with the increasing trend of electricity market price difference and the decrease in the costs of BESS [7]. In another paper, a net present value term is put forward. The net present value specifies that the worth of money spent today and money spent during the project period are not the same. This study also takes into account the cost reduction rate of BESS. A bi-level optimization method is applied in this paper. BESS location and capacity sizing are found in the outer loop of optimization by minimizing the net present value. Inner optimization rearranges the BESS size considering the investment cost of battery and battery lifetime [8]. It is noticed that the cost reduction rate of BESS reserves a crucial place to make an investment plan. In other work, a three-stage calculation procedure is used. In the first level, candidate locations and capacity values are determined by simulating several possible capacities for each day in a year. In the following stage, locations are fixed, and size adjustments are being made. Finally, an operation strategy is created for the storage system management with the fixed BESS size and location. Analysis performed on IEEE RTS 96 test case

to verify the proposed algorithm in this paper [9]. In another study, Shafiq and Khan suggest that usage of voltage sensitivity index method is an effective solution to obtain optimum BESS location and capacity. Voltage sensitivity index is calculated with dV/dP and dV/dQ Jacobian terms. This operation gives the buses that are most sensitive to voltage changes. In this paper, a 14-bus test system is chosen for demonstration. After solving the voltage sensitivity index, possible BESS locations appear. At the end of the study, sizing determination is done by checking out BESS output power versus bus voltage graph [10]. The first article about using the sensitivity analysis method for capacitor placement was published in 1994 [11]. Since the capacitor is a reactive power element, sensitivity analysis is made by taking the derivative of the real power losses with respect to the reactive power. Many papers published until now have cited this article that was published in 1994. In the following years, another paper was published about shunt capacitor placement using the loss sensitivity index method [12]. In this paper, sizing of the capacitor was found by particle swarm optimization technique targeting loss minimization. Another study compares loss sensitivity and bus sensitivity methods for capacitor placement. Loss sensitivity is calculated by derivation real power losses with respect to the reactive power. On the other hand, the bus sensitivity method uses bus voltages and reactive power. In this work, an objective function is formed to get minimum power losses and achieve maximum financial savings [13]. Optimal capacitor placement by using loss sensitivity index method was also verified in another study published in 2012 [14]. In the first stage of this study, real power loss sensitivity with respect to reactive power is considered for capacitor placement. However, a method called power loss index is described for capacitor sizing. Different sizes of capacitor values were placed on each bus and sorted according to their effects on the system. This process is repeated at different time intervals, and the capacitor that had the most effect on power losses is chosen. Karanki et al. [15] studied the loss sensitivity index for the allocation of the battery storage system. This paper uses the IEEE 34-Bus test case, which is an unbalanced distribution system. Separate sensitivity index calculations are made for each phase since the unbalancing issue. Then again, BESS

sizing is done by using loss minimization. The same authors released a paper in 2017, which is a modified version of their previous study. In their following study, a BESS controller algorithm is added to recent work that includes renewable generation output compensation. It is noticed that the mentioned BESS controller architecture is presented in the study of Brekken and Yokochi [16].

In all of the studies reviewed so far, it is taken into account that BESS only contributes to power generation. BESS is a device that has two modes of operation. This device can act as a load during the charging process and support generation when discharging. Hence, a methodology that considers both of these modes would give more accurate results.

In order to handle this issue, loss sensitivity factor calculations are made separately during all charging and discharging hours. The average of the loss sensitivity factor values calculated during the charging period is subtracted from the average of the loss sensitivity factor values obtained during the discharge period. This difference is called as Δ LSF, and optimum BESS location can be found by choosing the bus that gives maximum Δ LSF [17], [18]. In the paper of Widjaja [17], BESS power and capacity ratings are assigned as constant. However, system power loss calculations are made for different capacity values in order to find out the optimum size of BESS in the study of Sardi et al [18]. In both papers, the active power losses of the power system on an hourly basis are calculated for each hour of a day. The summation of these hourly-based losses gives daily losses of the system. According to these papers, daily losses will be reduced by using BESS.

Studies described so far suggest methods to determine optimal BESS placement in detail. However, suggested methods require an enhancement to cover the energy storage system pricing parameters. Energy capacity cost, power conversion cost, balance of plant cost, construction cost, operation and maintenance cost, round-trip efficiency, depth of discharge, and floating life of BESS parameters are presented in the guide of Eyer and Corey [19]. In other studies, similar BESS pricing parameters are proposed and described in detail to find the BESS investment cost [20], [21].

Nevertheless, these studies do not offer techniques for optimum placement of energy storage systems.

In this thesis, cost-benefit analysis is applied to provide an insight for energy storage system investors. The cost-benefit analysis is performed to find out the size of BESS. This analysis aims to cover the investment cost of BESS from the savings obtained by energy trading. Energy trading is done by taking advantage of the difference in electricity prices during the day. The optimum BESS placement is done by using the Δ LSF method. Consequently, this thesis study provides an approach for finding the optimum BESS location and assessing BESS size.

1.2 Thesis Outline

This thesis work consists of five chapters. Literature review and previous studies on the thesis subject are examined in the first chapter.

In second chapter, basic information about the terms used in the thesis and derivation of formulas are given. The historical process is explained, beginning from the discovery of batteries to the capacity improvements that can be used in power systems. The concept of microgrid, variable electricity pricing, daily load curve, and usage areas of BESSs are described. In the following sections, construction of network matrices, power flow calculation, and derivation of incremental transmission loss are expressed. Finally, loss sensitivity factor calculation is elaborated, which will be used for finding the optimum BESS location.

Chapter 3 presents the problem formulation and methodology. The first part of this chapter explains the relationship between loss sensitivity factor calculation and optimum battery placement. In the following part of this chapter, a cost-benefit analysis procedure is presented for pricing the BESS investment, including lifetime, cycle aging, depth of discharge parameters.

In Chapter 4, proposed methodologies are implemented with tests. IEEE 14-Bus, 9-Bus, and IEEE 33-Bus systems are chosen as the test cases. In this section,

simulations are performed to find the optimum BESS placement on these test cases. In addition, a cost-benefit analysis is performed to determine the size of the battery system, taking into consideration savings obtained from electricity trading and reduced losses.

The last chapter underlines the conclusions of this thesis and future developments that can be done to this study.

CHAPTER 2

BACKGROUND REVIEW

2.1 Electrical Grid

Electrical grid is an infrastructure that provides the generated electricity to the demand regions with the necessary protection and control mechanisms. Electricity generation is achieved by converting energy that exists in another form to the electrical energy. Simple version of an electrical grid can be observed from Figure 2.1.

Power plants operating with fuel or reserves such as hydroelectric, thermal, geothermal, natural gas can be given as examples of generation facilities. In addition to these facilities, there are renewable energy power plants connected to natural resources such as wind energy and photovoltaic, which can produce variable output.

The generated electricity is transferred to the demand areas by using transmission system. The basic elements of the transmission system are high voltage transmission lines, transformers and protection elements. Electricity transmission in Turkey is provided by 154 kV 3-phase and 400 kV 3-phase lines.

The distribution term is used for the process of transferring the delivered electricity to the demand zones to each customer. It will be uneconomic to distribute the electricity with high voltage systems and high voltage infrastructure. Therefore, the infrastructure suitable for low voltage level is used for distribution systems. In Turkey, the electricity received from the transmission system is reduced to 33.6-34.5kV 3-phase levels. This level is the highest voltage level at the distribution system in Turkey. The voltage level brought to the customer is reduced to 400V 3-phase and 230V monophasic by using transformers.

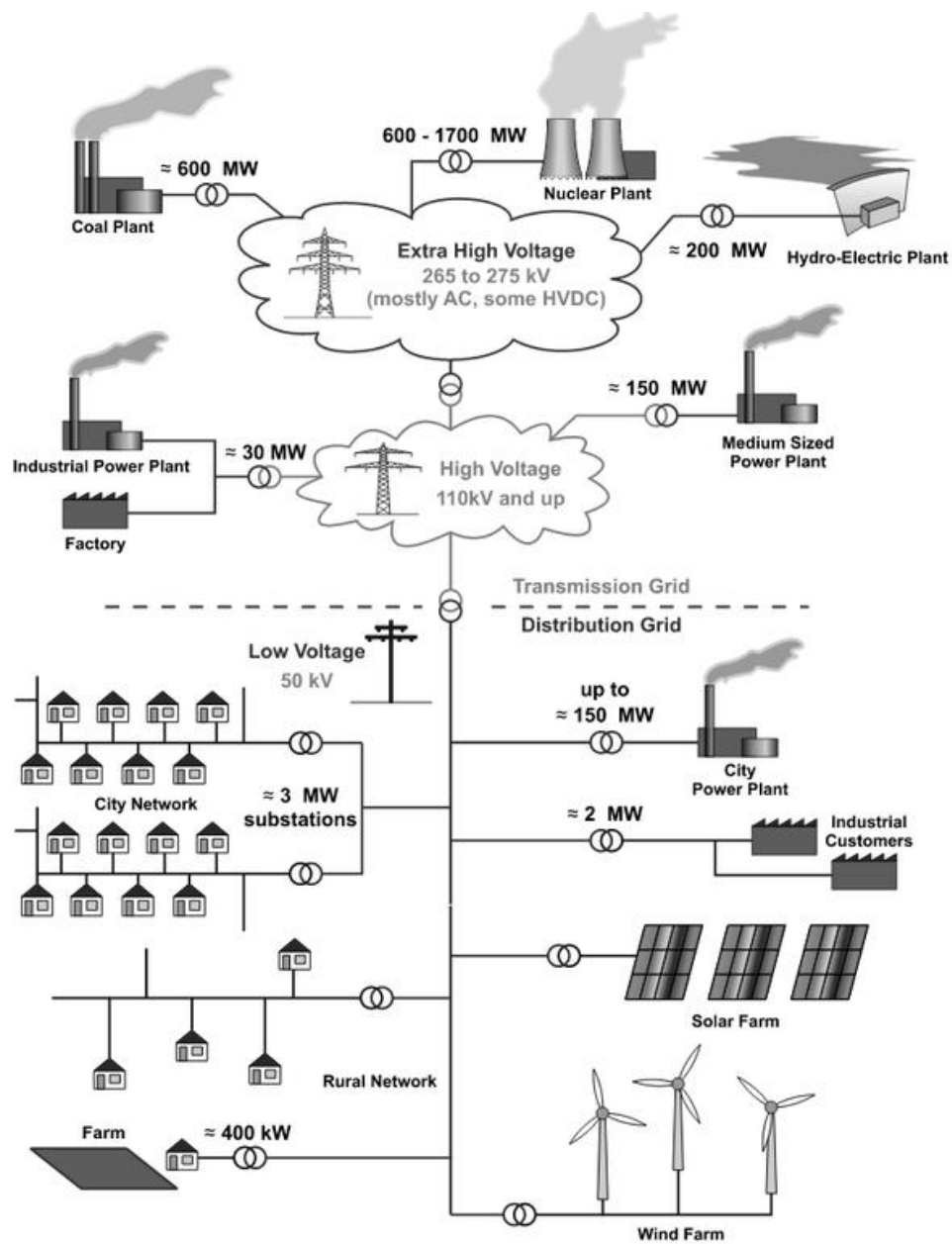


Figure 2.1. Basic Model of Electrical Grid [22]

2.2 Daily Load Curve and Load Shifting

The daily load curve is a graph of the load values demanded in a power system during the day. This curve can be prepared by using different time intervals, but it is generally given on an hourly basis.

The daily load curve can be quite different from each other depending on the time intervals, such as weekdays, weekends, and public holidays. Electricity demand varies depending on seasonal changes. In general, people use equipment that draws also electrical power, such as air conditioners, and human activity is more in summer periods. Although there is less mobility in winter, electricity usage is higher due to the need for heating and lack of daylight. However, the load demand in the winter season remains below of the summer season load. In autumn and spring, electricity consumption reaches minimum levels on average. Nevertheless, the spring season is considered as minimum. Consequently, three main daily load curve classifications can be made according to the seasons, as a summer peak, winter and spring minimum.

Figure 2.2 shows a sample daily load curve which is taken from Energy Exchange Istanbul (EXIST) [23]. This curve corresponds to the whole country's load demand of Turkey for the date 29.07.2019. The given curve is a combination of industrial and residential loads. Generally, the shape of this curve will be typical for other countries if the same combination is ensured. When the figure is examined, load demand decreases at midnight hours. It is also observed that the total demand increases during the daytime. In this thesis, the typical daily load curve of the country will be used by taking into account seasonal varieties. The hourly load demands of the tested power systems will be found by using the daily load curve in this study.

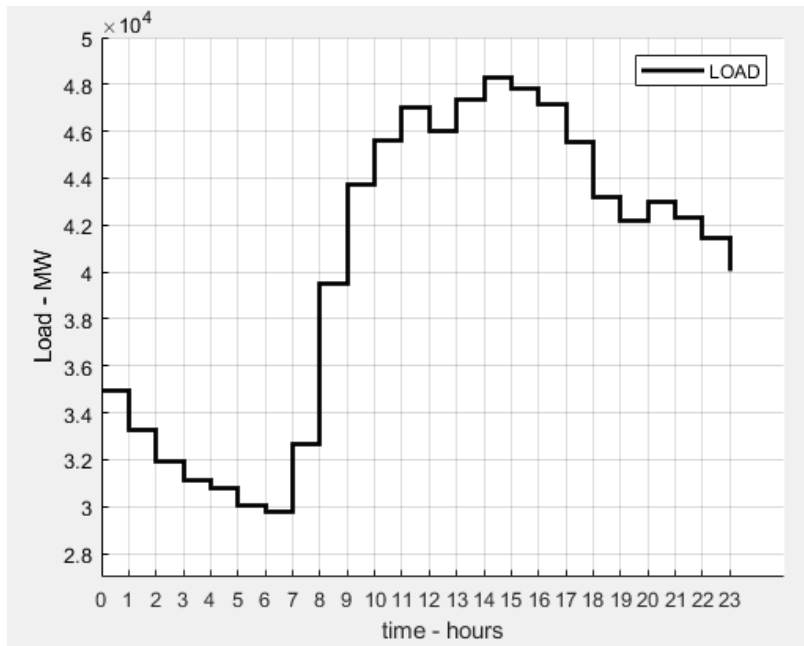


Figure 2.2. Turkey's Daily Load Curve for the Date 29.07.2019, Source: Energy Exchange Istanbul [23]

In general, it is desired that the shape of the daily load curve should be similar to a straight line. However, due to the daily life activities the straight-line case is impractical, and the typical form of the daily load curve will be come forward. The process of transporting the energy from this peak area to the off-peak area as much as possible is called valley filling or load shifting. Suppose that peak demand occurs for several hours of the day and the total load demand is low for the rest of the day in a power system. Units such as gas power plants and oil-fired steam generators are put into operation during peak load demand periods. These generation units are called peaker plants. A peaker plant generates electricity at a higher price rate than the generation price of off-peak hours. Therefore, giving generation orders to these plants is financially disadvantageous. In addition, comparably expensive infrastructure arrangements should be made for these power generation units. This is because transmission lines need to be upgraded for these peak loads that occur at certain hours. Operation and maintenance costs also advance up due to the peak power. For these reasons, load shifting has an essential role in power systems. BESSs

have started to establish a market presence for load shifting applications with improved capacity rating values [24].

2.3 Evolution Process of Batteries

Luigi Galvani was the first to discover that electricity could be produced with a chemical reaction. Physicist Alessandro Volta developed the first working prototype of the battery in the early 1800s with the help of Galvani's work. This simple battery produced by Volta was named after the voltaic battery. The voltaic battery consists of gluing the zinc and silver parts on each other and stacking these zinc-silver pairs in a solution liquid. Michael Faraday discovered the laws of electrolysis by working on the battery developed by Volta. Faraday's laws show the relationship between the electrode material forming the battery and the resulting electric power. Later, John Frederic Daniell produced a battery that performed better than the Voltaic battery in continuous operation by using zinc and copper in sulfuric acid. In 1839, William Robert Grove produced a battery containing a platinum cathode, sulfuric acid, and nitric acid. After that, Robert Wilhelm Bunsen used less costly carbon instead of the platinum in Grove's battery.

In 1859, Gaston Plante invented lead-acid cells, one of the battery types widely used in the world today. This battery is recognized as the first storage battery model. Lead-acid batteries have the ability to provide more current than their competitor. Alkaline batteries were developed between the late-1800s and early-1900s. Alkaline-type batteries are frequently preferred by consumers, such as rechargeable Nickel-Cadmium batteries. In the mid-1900s, zinc-silver oxide type batteries were produced, which were the best in terms of energy provided per unit volume. For the last 60 years, rapidly developing technology has contributed to significant developments in the battery sector since electronic devices have become indispensable in consumer electronics. Today, lithium batteries find their place in the market with a dominant effect. Lithium-type batteries are used in electric vehicles and BESS applications, which have become one of the most popular topics in recent years [25].

A primary battery is a battery used once and discarded after emptying. On the other hand, a secondary battery is a battery that can be charged and discharged many times before being thrown away. Secondary batteries, as a matter of course, have a limited lifespan. Secondary batteries, also known as storage batteries, can be produced in many different compositions and types. Depending on the battery type, the number of charge-discharge cycles may vary.

Rechargeable batteries supply DC current. In discharging mode, electron flow is provided to the connected device with the voltage difference formed on the battery electrodes. In charging mode, when a DC voltage is applied to the electrodes opposite to the discharge direction of the battery more than the battery's voltage, the electrons return to their place before the discharge with the battery's chemistry. In each cycle of these reactions, the battery's life weakens, and the battery's actual capacity decreases.

The lead-acid battery is one of the most common secondary batteries with mobility skills. Automobile accumulator battery is the most known example of lead-acid type batteries. This type of storage device consists of lead sulfate and sulfuric acid. It is commonly preferred due to its long shelf life and the high number of charge cycles such as hundreds of times.

Alkaline storage batteries can be shown as another type of secondary battery. It can be an ideal solution in portable devices for low current and voltage conditions. There are many alkaline batteries such as nickel-cadmium, nickel-zinc, nickel-iron, nickel-hydrogen.

Lithium-type batteries have had a very high share in the sector in recent years. Lithium-metal type batteries have an energy density of 2000 Watt-hours/kg. These types of batteries are better for safety issues. Today, high investments are made in this type of battery and developing rapidly [25]. Li-ion batteries have been widely used since the early 1990s. Li-ion batteries are frequently preferred due to their high efficiency and prolonged charging cycles. Although they have high values in terms

of charge cycles, Li-ion batteries have a lower life span. The self-discharge level of Li-ion batteries is also very low [26].

Considering the distribution of battery energy storage systems installed today, Li-ion batteries have a market share of 78%. Furthermore, 74% of the planned projects use the Li-ion battery type. Li-ion batteries are one of the fastest developing battery types with the widespread use of electric vehicles [27].

The use of energy storage systems in power systems has become a prominent issue in recent years, with the ability to operate at high currents and powers. Many types of battery technologies are used in the world for energy storage. As of the beginning of 2021, 1300+ Energy storage projects are being carried out according to DOE Global Energy Storage Database data. The capacities of these systems have reached 174 GW, and they are operational. In addition, 330+ energy storage system projects are currently underway [27]. As a result of the decrease in the production of fossil fuels over time and the consumption of resources, the need for alternative energy sources has arisen. Indeed, the increase in environmental concerns forces fossil fuels to be replaced by more environmentally friendly solutions. These reasons have been a factor that accelerated the process of using batteries as an energy storage system [26].

With the technological developments experienced, there are dramatic changes in power systems. Systems have been developed to generate electricity when necessary and draw an electrical load when the opposite condition occurs. Such systems are called prosumers. These systems work with electricity storage units and provide an economic contribution by using variable electricity prices [28].

2.4 Time of Use Pricing

In the mid-20th century, a three-rate tariff system for electricity prices is offered to customers as an option in some countries. Before that, a single tariff system was being used, which charges customers at a fixed price proportional to the consumption

[29]. The main purpose of the three-rate tariff is that spread the load demand to the hours other than peak load occurs. Since electricity prices are higher during peak hours, consumers are encouraged to choose other hours.

Nowadays, intraday electricity pricing is being used which participants can exchange contracts. The trend is toward spot prices that provide better flexibility to market players and individuals. Recently, individuals can use remote devices with the help of Internet-of-Things technology. An individual can decide remotely to use electrical appliances, such as electric vehicle charging, by checking out spot prices in real-time.

In this study, hourly electricity price snapshots are taken. In the scope of this work, it is assumed that BESS is an active member of the grid by charging or discharging electricity at the price rate related hour.

Today, electricity market management applications improve rapidly. The smart-grid concept accelerates this improvement. Smart-grid is defined as an electricity grid integrated with digital communication technologies, which enables participants to play an active role. Smart-grid contains several power producers that can be independent of governments. BESS is an ideal component that suits the Smart-grid concept.

2.5 Distributed Generation, Microgrids and Load Shedding

Gas turbines, fuel cells, renewable sources such as wind turbines, and photovoltaic can be connected each other to supply loads in small local areas. These generation sources are called Distributed Energy Resources (DER). Loads with DERs in this small field can form a grid relatively small size called Microgrid. Microgrids must be connected to the grid, disconnected from the grid, and operate independently of the grid [30]. The connection to the grid is usually made through a single point, called the point of common coupling (PCC). When microgrids operate independently of the grid, it is called island mode.

Microgrids aim to minimize costs by controlling the elements at the optimum level. Considering the variable outputs of renewable sources that microgrids contain, BESSs can compensate this uncertainty. The integration of BESSs with microgrids plays a significant role in cost minimized operations. Governments also support the propagation of microgrids. In this way, consumers meet their own electricity needs by using the system network at a minimum level. In addition, due to the structure of microgrids, new technologies such as renewable sources and BESS affect the environmental concern positively. Microgrids help to reduce power losses and increase reliability [30]. However, it has adverse effects on grid security and power system stability. An illustration of a microgrid with a storage system is given in Figure 2.3.

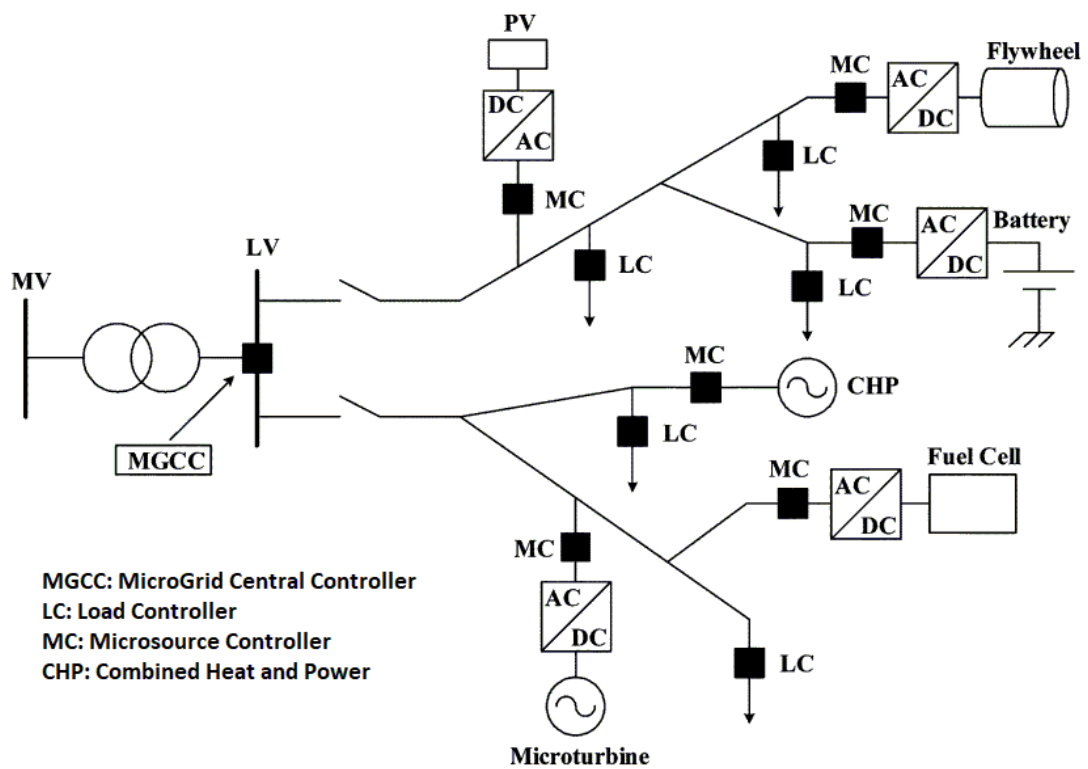


Figure 2.3. A Sample Microgrid System that has an Energy Storage Unit [31]

For microgrids to be cost-effective, the capacity and power of BESSs located in the grid are essential. The production cost of BESSs also affects the value of these parameters linearly. Therefore, optimum BESS sizing and power calculations are required for a cost minimized solution. Microgrids are built in a small area by their nature, and therefore BESS's bus location will have a negligible effect.

Disturbances such as faults in the power system can cause disconnection of loads. If the system frequency drops due to disturbances, it is ensured that a group of loads are removed with under-frequency relays, and/or the generators are out of the circuit. High stresses occur on the parts of generators with moving parts at low frequencies, and these parts are damaged. For this reason, the system frequency is monitored, and critical levels are determined. Frequency drop values are determined at different stages, and the amount of load to be shed is specified. A step-by-step shedding operation is applied when there is a frequency drop with the determined load shedding scheme. It is aimed to restore the system after load shedding. In this way, the system can be restored without irreversible faults [32].

Small systems can arise due to load shedding, which is isolated from the main power system. These systems are called islands which can involve generators. Evidently, load shedding operation can be applied to microgrids. If an island has a generator, this island will be tried to be powered by that generator. In an islanded region with under-frequency load shedding, it is possible to maintain the electricity supply by using BESS. Instead of feeding the entire islanded region from BESS, an effective method can be followed, such as determining critical loads that may be vital in case of power loss and feeding these areas with BESS. The study [33] shows that the BESSs can be used as a primary frequency control unit. Moreover, it is stated in this study that batteries are also used for peak shaving.

2.6 Application Benefits That Motivate the Usage of BESS

2.6.1 Exploiting Variations in Electrical Energy Price

Electrical energy prices in either intraday or day-ahead market are variable in a day due to the supply and demand competition. Energy prices are generally low when the demand is low, i.e., after midnight hours. In contrast, the highest prices in the energy market typically occur close to the evening hours of the day. Taking advantage of this price difference by using BESS provides benefits both economically and operationally. It is possible to benefit from the price difference by charging BESSs during low electricity prices and discharging BESSs when electricity prices are high [34]. Financial benefits can be obtained from peak shaving and load shifting applications by making electricity trading.

2.6.2 Load and Generation Support

Load-generation balance forms the basis of the management of power systems. The system operator adjusts the electricity generation by determining and predicting the loads in the next hour. For this application, the amount to be produced in the next hour is ordered to the power plants to aim electricity production at minimum cost. Using BESSs by discharging them to the grid when there is more load demand than production and charging from the power system when the generation is more than the load will contribute to the load-generation balance [34].

2.6.3 Operating Reserves

Operational spares are the name given to the backups that can provide electricity production for a certain period by taking over the lost unit's place if the generator unit fails. Generator units that are ready to be connected to the system are also operated beside the generator units that are already online. These reserve units are in

operation with no-load, and they are known as hot reserves. BESSs can be used as spinning hot reserves with response times in the order of seconds [27]. Apparently, keeping an extra generator, costs more than the total cost of the BESS.

2.6.4 Black Start

As an old-fashioned method, diesel generators are used for black start operation. BESSs are rarely used as a black start service. Especially in system-wide blackouts, generation plants have to make their first commissioning by drawing electricity from the grid. Black start operation can be performed with the help of BESSs.

The electricity grid has two main tasks to perform. These are the electricity production according to the supply and the delivery of the produced electricity to the supply points. Ancillary services are support applications made to assist the transportation of this electricity produced to customers in reliable, satisfying power quality and considering grid constraints [34].

Black start and spinning reserves are a type of ancillary services. The potential types of ancillary services that BESSs can be used and their explanations are given in Table 2.1 [19].

Until now, widely used application areas of BESS have been described. The other potential application types of BESS related to ancillary services are given in Table 2.1. In this thesis, the main objective is to reach a breakeven point that provides earnings by implementing an energy trading application using BESS. Evidently, there are investment and operation costs of BESS, and the mentioned breakeven point implies that BESS would financially return its investment expenses in the lifetime of the battery by taking advantage of hourly price differences in an energy market. The applied approach in this thesis also contributes to the load shifting purpose.

Table 2.1. The Potential Types of Ancillary Services that
Can be Used for BESS Applications [19]

System Control and Regulation	Load-generation balance tracking in frequent time intervals to comply with system rule-makers standards
Operation Reserves	Frequency triggered operation reserves for rapid reaction instead of using old-fashioned slow hot reserves
Supplemental Reserve	Supply the load curtailed regions for a certain amount of time
Power Loss Reduction	Decrease the system power losses in transmission and distribution lines by supplying the generation
Black Start	Supporting start-up of generators to get back alive the system which is entirely collapsed
Grid Stability	Giving the counter-response to the disturbances to keep the system stability in the safe region
Load Tracing	Satisfying hourly load demands by tracing the loads given in the daily load curve

2.7 Network Matrices

2.7.1 Bus Admittance Matrix

Bus admittance matrix is formed by using the relation between the injected currents and node voltage [35]. The bus admittance matrix is built by performing nodal analysis at steady-state. Bus admittance matrix is a super sparse matrix; hence computational techniques should be performed to speed up the computer analysis. The branch term is used for the component connected to the network. The branch is defined as the component connected to a reference node or component connected between two nodes. The relationship between bus admittance matrix (\mathbf{Y}_{bus}), current

injection vector (\mathbf{I}) at related nodes, and node voltage vector (\mathbf{V}) are given as following equation.

$$\mathbf{I} = \mathbf{Y}_{\text{bus}} \cdot \mathbf{V} \quad (2.1)$$

Bus admittance matrix is symmetric if there is no phase-shifting element on the network. \mathbf{Y}_{bus} is non-singular if there are one or more connections to the ground on the network.

Construction steps of the bus admittance matrix are given as follows. Assume that the system has two buses represented with i and j terms. Y_{ii} equals to the sum of all admittances between Bus- i and other buses connected to Bus- i . Y_{ij} equals to sum of negative of all admittances between Bus- i and Bus- j . If there is more than one branch is parallelly connected between Bus- i and Bus- j then the equivalent admittance of these elements should be calculated first.

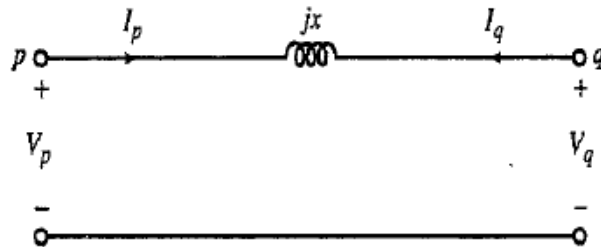


Figure 2.4. Basic Circuit Model of a Transformer [36]

Bus admittance matrix of this model is shown in Equation 2.2 by applying the methods explained above.

$$\begin{bmatrix} I_p \\ I_q \end{bmatrix} = \begin{bmatrix} \frac{1}{jx} & \frac{-1}{jx} \\ \frac{-1}{jx} & \frac{1}{jx} \end{bmatrix} \begin{bmatrix} V_p \\ V_q \end{bmatrix} \quad (2.2)$$

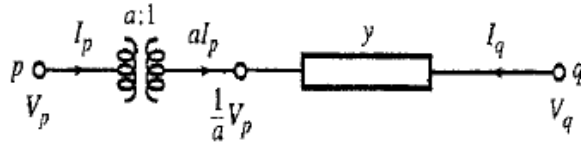


Figure 2.5. Diagram of a Transformer that has an Off-Nominal Turns Ratio [36]

Bus admittance matrix of off-nominal turns ratio version of a transformer can be found using Figure 2.6. The following equation is found by modifying Equation 2.2 with branch admittance (y) and turns ratio (a).

$$\begin{bmatrix} aI_p \\ I_q \end{bmatrix} = \begin{bmatrix} y & -y \\ -y & y \end{bmatrix} \begin{bmatrix} \frac{1}{a}V_p \\ V_q \end{bmatrix} \quad (2.3)$$

The matrix equation below is attained by performing matrix operations to Equation 2.3.

$$\begin{bmatrix} I_p \\ I_q \end{bmatrix} = \begin{bmatrix} \frac{y}{a^2} & -\frac{y}{a} \\ -\frac{y}{a} & y \end{bmatrix} \begin{bmatrix} V_p \\ V_q \end{bmatrix} \quad (2.4)$$

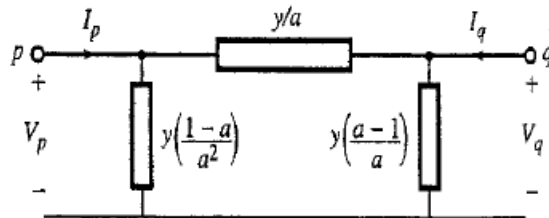


Figure 2.6. Circuit Model of a Transformer that has an Off-Nominal Turns Ratio [36]

2.7.2 Bus Impedance Matrix

Forming the bus impedance matrix (Z_{bus}) is more challenging than the bus admittance matrix considering computational burden. Bus impedance matrix is a favorable choice for short circuit calculations. Z_{bus} is the inverse of Y_{bus} matrix.

$$V = Z_{bus} \cdot I \quad (2.5)$$

Z_{ij} gives the open circuit driving point impedance if bus number i equals to j . On the other hand, if bus numbers i and j are non-equal, Z_{ij} gives the open circuit transfer impedance. The following characteristics should be considered for the construction of bus impedance matrix. Z_{bus} is a symmetric matrix. Bus impedance matrix is not a sparse matrix contrary to bus admittance matrix. Hence, it is expensive to store Z_{bus} matrix considering the computational burden. Diagonal element of Z_{bus} gives Thevenin impedance of the system. Directly construction of the bus impedance matrix is more problematic considering time and resource since it contains several matrix modifications steps. Hence, in this thesis, bus impedance matrix of a system will be found by inverting Y_{bus} matrix as described in Equation 2.6.

$$Z_{bus} = Y_{bus}^{-1} \quad (2.6)$$

2.8 Power Flow Analysis

Power flow analysis is crucial for power systems at the beginning of the construction plan and during the operation of the grid. Power flow studies give us active-reactive power flows and voltage angle-magnitudes for each bus. Performing basic methods for these calculations is not practical, considering time limits. Hence, computer technologies are being used for power flow analyses.

There are several methods to simplify and speed up the calculation process. The Gauss-Seidel Method and The Newton Raphson Method are the most common methods to solve power flow equations [36].

Both the bus admittance matrix and the bus impedance matrix can be used to solve a power flow problem. However, Y_{bus} is used to solve power flow problems in this thesis work. Note that the subscript i refers to Bus- i , k refers to Bus- k , Y_{ik} is an element of the bus admittance matrix. Per phase bus power (S_i) is used for the calculations. The number of buses in a power system is denoted by n . S_i is the net complex power injection at Bus- i into the network. It is equal to the sum of complex power flowing from Bus- i to neighboring buses.

$$S_i = \sum_{k=1}^n S_{ik} \quad i = 1, 2, 3, \dots, n \quad (2.7)$$

Similarly, net current injection at node i (I_i) can be expressed as follows.

$$I_i = \sum_{k=1}^n I_{ik} \quad i = 1, 2, 3, \dots, n \quad (2.8)$$

Hence,

$$I_i = Y_{i1}V_1 + Y_{i2}V_2 + \dots + Y_{in}V_n = \sum_{k=1}^n Y_{ik}V_k \quad i = 1, 2, 3, \dots, n \quad (2.9)$$

Equation 2.10 below gives the net complex power at Bus- i (S_i) in terms of bus voltages.

$$S_i = V_i I_i^* = V_i \sum_{k=1}^n (Y_{ik}^* V_k^*) \quad i = 1, 2, 3, \dots, n \quad (2.10)$$

$$V_i \triangleq |V_i| e^{j\theta_i} \quad (2.11)$$

$$\theta_{ik} \triangleq \theta_i - \theta_k \quad (2.12)$$

$$Y_{ik} \triangleq G_{ik} + jB_{ik} \quad (2.13)$$

Bus voltage (V_i) is given as polar coordinates in Equation 2.11, and rectangular representation is used for bus admittance element (Y_{ik}) in Equation 2.13. G_{ik} and B_{ik} are known as conductance and susceptance, respectively. Equation 2.14 is found after modification of Equation 2.10.

$$\begin{aligned} S_i &= \sum_{k=1}^n |V_i| |V_k| e^{j\theta_{ik}} (G_{ik} - jB_{ik}) \quad (2.14) \\ &= \sum_{k=1}^n |V_i| |V_k| (\cos \theta_{ik} + j \sin \theta_{ik}) (G_{ik} - jB_{ik}) \quad i = 1, 2, 3, \dots, n \end{aligned}$$

Splitting into complex parts of Equation 2.14 gives the following two equations.

$$P_i = \sum_{k=1}^n |V_i| |V_k| (G_{ik} \cos \theta_{ik} + B_{ik} \sin \theta_{ik}) \quad (2.15)$$

$$Q_i = \sum_{k=1}^n |V_i| |V_k| (G_{ik} \sin \theta_{ik} - B_{ik} \cos \theta_{ik}) \quad (2.16)$$

Net active (P_i) and reactive (Q_i) power injections at Bus- i can be obtained by using Equations 2.15 and 2.16.

There are four variables associated with each bus, as can be noticed by examining Equation 2.15 and Equation 2.16. These variables are $|V_i|$, δ_i , P_i and Q_i . Due to the characteristic of the power system, two of these four variables are known for each bus. Unknown remaining ones can be calculated with the method of power flow. Power system bus types can be categorized as follows:

Slack Bus: This bus is also known as the swing bus. In general, slack bus voltage angle is chosen as 0° . Hence, all other bus voltage angles are referenced to this bus.

PV Bus: PV buses are known as voltage-controlled buses. The active power of generation on these buses is also controllable. Hence, P_i and $|V_i|$ are knowns and Q_i , δ_i are unknowns.

Load Bus: In other words, they are named as a PQ bus. If the system has no generator at a bus, then type of this bus is a load bus. These buses draw active and reactive power from the system. The unknown variables are $|V_i|$, δ_i .

2.8.1 Newton Raphson Method

Newton-Raphson method uses linear approximation approach to find the roots of a non-linear function. Equation 2.17 is the formula of the one-dimensional Newton-Raphson method.

$$x^{v+1} = x^v - [f'(x^v)]^{-1}f(x^v) \quad (2.17)$$

This is an iterative method, and the solution converges to the desired value after each iteration. Iteration counter is denoted by v .

Equation 2.17 can be expanded to multi-dimensional case. To do that, Taylor expansion is used [35]. One-dimensional Taylor series expansion is given in Equation 2.18.

$$f(\mathbf{x} + \Delta\mathbf{x}) = f(\mathbf{x}) + f'(\mathbf{x})\Delta\mathbf{x} + \text{h. o. t.} \quad (2.18)$$

Instead of writing higher-order terms, they are represented by h.o.t. notation. Note that n is the dimension number, and bold character is chosen for multi-dimensional vectors. Equation 2.18 can be modified to n dimensional case as given in Equation 2.19.

$$\begin{aligned} f_1(\mathbf{x} + \Delta\mathbf{x}) &= f_1(\mathbf{x}) + \frac{\partial f_1(\mathbf{x})}{\partial x_1} \Delta x_1 + \dots + \frac{\partial f_1(\mathbf{x})}{\partial x_n} \Delta x_n + \text{h. o. t.} \quad (2.19) \\ f_2(\mathbf{x} + \Delta\mathbf{x}) &= f_2(\mathbf{x}) + \frac{\partial f_2(\mathbf{x})}{\partial x_1} \Delta x_1 + \dots + \frac{\partial f_2(\mathbf{x})}{\partial x_n} \Delta x_n + \text{h. o. t.} \\ &\cdot \\ &\cdot \\ f_n(\mathbf{x} + \Delta\mathbf{x}) &= f_n(\mathbf{x}) + \frac{\partial f_n(\mathbf{x})}{\partial x_1} \Delta x_1 + \dots + \frac{\partial f_n(\mathbf{x})}{\partial x_n} \Delta x_n + \text{h. o. t.} \end{aligned}$$

In the next stage, these equations can be converted to matrix representation as follows.

$$f(\mathbf{x} + \Delta\mathbf{x}) = f(\mathbf{x}) + \mathbf{J}(\mathbf{x})\Delta\mathbf{x} + \text{h. o. t.} \quad (2.20)$$

It is evident that Equation 2.20 is an updated version of Equation 2.18 for n dimensional case.

$$\mathbf{J}(\mathbf{x}) \triangleq \begin{bmatrix} \frac{\partial f_1(\mathbf{x})}{\partial x_1} & \cdots & \frac{\partial f_1(\mathbf{x})}{\partial x_n} \\ \vdots & & \vdots \\ \frac{\partial f_n(\mathbf{x})}{\partial x_1} & \cdots & \frac{\partial f_n(\mathbf{x})}{\partial x_n} \end{bmatrix} \quad (2.21)$$

$$\Delta \mathbf{x} \triangleq \begin{bmatrix} \Delta x_1 \\ \Delta x_2 \\ \vdots \\ \Delta x_n \end{bmatrix} \quad (2.22)$$

Equation 2.21 contains all first-order partial derivatives of the function, also known as the Jacobian matrix (\mathbf{J}). To finalize the derivation of n dimensional Newton-Raphson method, Equation 2.23 is created by using Equations 2.17, 2.18, and 2.20.

$$\mathbf{x}^{v+1} = \mathbf{x}^v - [\mathbf{J}(\mathbf{x}^v)]^{-1} \mathbf{f}(\mathbf{x}^v) \quad (2.23)$$

As observed from Equation 2.23, Jacobian Matrix needs to be updated for each iteration. Inverse of the Jacobian Matrix should be taken. This operation is heavy for computational burden. A reorganized version of Equation 2.23 is shown in Equations 2.24 and 2.25 to avoid getting inverse of Jacobian.

$$\Delta \mathbf{x}^v \triangleq \mathbf{x}^{v+1} - \mathbf{x}^v \quad (2.24)$$

$$-\mathbf{J}^v \Delta \mathbf{x}^v = \mathbf{f}(\mathbf{x}^v) \quad (2.25)$$

2.8.2 Power Flow Calculation Using Newton Raphson Method

Equations 2.15 and 2.16 are used for the power flow analysis using Newton Raphson Method. Suppose that, θ_1 and V_1 are known. Hence, the index numbering starts from 2. The following equation gives vector matrices of bus angles and voltages [35].

$$\boldsymbol{\theta} = \begin{bmatrix} \theta_2 \\ \theta_3 \\ \vdots \\ \theta_n \end{bmatrix} \quad |\mathbf{V}| = \begin{bmatrix} |V_2| \\ |V_3| \\ \vdots \\ |V_n| \end{bmatrix} \quad \mathbf{x} = \begin{bmatrix} \boldsymbol{\theta} \\ |\mathbf{V}| \end{bmatrix} \quad (2.26)$$

Equation 2.26 shows that, the right side of Equations 2.15 and 2.16 are function of 2.26. Hence, the updated version of Equations 2.15 and 2.16 are given as follows.

$$P_i(\mathbf{x}) \triangleq \sum_{k=1}^n |V_i| |V_k| (G_{ik} \cos(\theta_i - \theta_k) + B_{ik} \sin(\theta_i - \theta_k)) \quad (2.27)$$

$$Q_i(\mathbf{x}) \triangleq \sum_{k=1}^n |V_i| |V_k| (G_{ik} \sin(\theta_i - \theta_k) - B_{ik} \cos(\theta_i - \theta_k))$$

The angle and voltage value of Bus-1 are known. Therefore, indexing starts from 2 in the bus power equations given below.

$$P_i = P_i(\mathbf{x}) \quad (2.28)$$

$$Q_i = Q_i(\mathbf{x}) \quad i = 2, 3, 4, \dots, n$$

Equation 2.28 shows us the left side of the equation is constant, and the right side is a function of \mathbf{x} . If the right side is subtracted from the left side, a mismatch will be found, and then iterative methods can be applied to see the value that converges the mismatch to 0.

$$\mathbf{f}(\mathbf{x}) \triangleq \begin{bmatrix} P_2(\mathbf{x}) - P_2 \\ \vdots \\ P_n(\mathbf{x}) - P_n \\ \text{---} \\ Q_2(\mathbf{x}) - Q_2 \\ \vdots \\ Q_n(\mathbf{x}) - Q_n \end{bmatrix} = 0 \quad (2.29)$$

In Equation 2.30, the Jacobian matrix is divided into parts.

$$\mathbf{J} = \begin{bmatrix} \mathbf{J}_{11} & \mathbf{J}_{12} \\ \mathbf{J}_{21} & \mathbf{J}_{22} \end{bmatrix} \quad (2.30)$$

Jacobian Matrix is represented by \mathbf{J} instead of $\mathbf{J}(\mathbf{x})$ for the convenience. \mathbf{J}_{11} contains terms related to $\frac{\partial P_i(\mathbf{x})}{\partial \theta_k}$, \mathbf{J}_{12} has the terms that correspond to $\frac{\partial P_i(\mathbf{x})}{\partial |V_k|}$, \mathbf{J}_{21} represents the terms related to $\frac{\partial Q_i(\mathbf{x})}{\partial \theta_k}$ and \mathbf{J}_{22} symbolizes the terms related to $\frac{\partial Q_i(\mathbf{x})}{\partial |V_k|}$.

Equation 2.31 is created by rearranging the Jacobian representation of the Newton-Raphson method using Equation 2.29, where v is the iteration counter.

$$\begin{bmatrix} \mathbf{J}_{11}^v & \mathbf{J}_{12}^v \\ \mathbf{J}_{21}^v & \mathbf{J}_{22}^v \end{bmatrix} \begin{bmatrix} \Delta \boldsymbol{\theta}^v \\ \Delta |\mathbf{V}|^v \end{bmatrix} = \begin{bmatrix} \Delta \mathbf{P}(\mathbf{x})^v \\ \Delta \mathbf{Q}(\mathbf{x})^v \end{bmatrix} \quad (2.31)$$

Mismatch vectors of active and reactive bus power are used in Equation 2.31. These vectors can be calculated from Equation 2.32.

$$\Delta \mathbf{P}_n(\mathbf{x}) = P_n - P_n(\mathbf{x}) \quad (2.32)$$

$$\Delta \mathbf{Q}_n(\mathbf{x}) = Q_n - Q_n(\mathbf{x})$$

The main purpose is to find the correct \mathbf{x}^v value, which gives zero mismatches for ΔP and ΔQ . Obviously, zero mismatches are not possible in general conditions. Hence, there is an acceptable error limit, and it should be satisfied.

\mathbf{x}^v matrix is given in Equation 2.26. To find next iteration $\Delta \mathbf{x}^v$ should be calculated. To pass subsequent iteration, use $\mathbf{x}^{v+1} = \mathbf{x}^v + \Delta \mathbf{x}^v$. After \mathbf{x}^{v+1} is found, update Equation 2.31. Jacobian terms, shown in Equation 2.30, are calculated as follows.

For matrix index $p \neq q$:

$$J_{pq}^{11} = \frac{\partial P_p(\mathbf{x})}{\partial \theta_q} = |V_p||V_q|(G_{pq}\sin \theta_{pq} - B_{pq}\cos \theta_{pq}) \quad (2.33)$$

$$J_{pq}^{21} = \frac{\partial Q_p(\mathbf{x})}{\partial \theta_q} = -|V_p||V_q|(G_{pq}\cos \theta_{pq} + B_{pq}\sin \theta_{pq})$$

$$J_{pq}^{12} = \frac{\partial P_p(\mathbf{x})}{\partial |V_q|} = |V_p|(G_{pq}\cos \theta_{pq} + B_{pq}\sin \theta_{pq})$$

$$J_{pq}^{22} = \frac{\partial Q_p(\mathbf{x})}{\partial |V_q|} = |V_p|(G_{pq}\sin \theta_{pq} - B_{pq}\cos \theta_{pq})$$

For matrix index $p = q$:

$$J_{pp}^{11} = \frac{\partial P_p(\mathbf{x})}{\partial \theta_p} = -Q_p - B_{pp}|V_p|^2 \quad (2.34)$$

$$J_{pp}^{21} = \frac{\partial Q_p(\mathbf{x})}{\partial \theta_p} = P_p - G_{pp}|V_p|^2$$

$$J_{pp}^{12} = \frac{\partial P_p(\mathbf{x})}{\partial |V_p|} = \frac{P_p}{|V_p|} + G_{pp}|V_p|$$

$$J_{pp}^{22} = \frac{\partial Q_p(\mathbf{x})}{\partial |V_p|} = \frac{Q_p}{|V_p|} - B_{pp}|V_p|$$

It can be observed from Equations 2.33 and 2.34; that Jacobian elements will be zero if there is no direct connection between the two buses. So, many Jacobian elements could be zero, and the computational load would reduce. This case is related to the bus admittance matrix. It is clearly an effective solution for larger power systems such as a large power system. Thousands of buses connected each other, and sparsity of Jacobian will enormously simplify solutions.

2.9 Transmission Loss Calculation

2.9.1 General Transmission Loss Formula

The transmission losses in a given system can be found by summing the net injected powers at all buses after solving the load flow problem. Equation 2.7 shows the injected active (P) and reactive (Q) powers at buses. Let us rewrite formula with different representation.

$$P_{\text{loss}} + jQ_{\text{loss}} = \sum_{i=1}^n S_i = \sum_{i=1}^n V_i I_i^* \quad (2.35)$$

Vector representation of Equation 2.35 is found using the inner matrix multiplication rule.

$$P_{\text{loss}} + jQ_{\text{loss}} = \mathbf{V}_{\text{bus}}^T \mathbf{I}_{\text{bus}}^* \quad (2.36)$$

$$P_{\text{loss}} + jQ_{\text{loss}} = \mathbf{I}_{\text{bus}}^T \mathbf{Z}_{\text{bus}}^T \mathbf{I}_{\text{bus}}^* = \mathbf{I}_{\text{bus}}^T \mathbf{Z}_{\text{bus}} \mathbf{I}_{\text{bus}}^* \quad (2.37)$$

To find Equation 2.37, corresponding terms of Equation 2.36 are replaced by using Equation 2.5.

Z_{bus} matrix can be broken into its components in Equation 2.38 which are resistance (\mathbf{R}) and impedance (\mathbf{X}) matrices.

$$\mathbf{Z}_{bus} = \mathbf{R} + j\mathbf{X} \quad (2.38)$$

By the same logic, split current vector into its components in the following equation.

$$\mathbf{I}_{bus} = \mathbf{I}_r + j\mathbf{I}_x \quad (2.39)$$

Equation 2.40 is a rearranged form of Equation 2.37 using the complex elements of bus current and bus impedance matrices.

$$S_{loss} = P_{loss} + jQ_{loss} = (\mathbf{I}_r + j\mathbf{I}_x)^T (\mathbf{R} + j\mathbf{X}) (\mathbf{I}_r - j\mathbf{I}_x) \quad (2.40)$$

Taking the real component of Equation 2.40 gives the following equation.

$$P_{loss} = \mathbf{I}_r^T \mathbf{R} \mathbf{I}_r + \mathbf{I}_r^T \mathbf{X} \mathbf{I}_x + \mathbf{I}_x^T \mathbf{R} \mathbf{I}_x - \mathbf{I}_x^T \mathbf{X} \mathbf{I}_r \quad (2.41)$$

In the following equation, Equation 2.41 simplifies since the second and the fourth components cancel out each other.

$$P_{loss} = \mathbf{I}_r^T \mathbf{R} \mathbf{I}_r + \mathbf{I}_x^T \mathbf{R} \mathbf{I}_x \quad (2.42)$$

Different expression of Equation 2.42 is shown as follows, where R_{ik} refers to ik^{th} element of Z_{bus} matrix.

$$P_{\text{loss}} = \sum_{i=1}^n \sum_{k=1}^n R_{ik} (I_{ri} I_{rk} + I_{xi} I_{xk}) \quad (2.43)$$

Usually, bus voltages are used for power system applications hence current vectors in Equation 2.43 should be translated to voltage ones.

$$P_i + jQ_i = V_i (I_{ri} - I_{xi}) = |V_i| (\cos \delta_i + j \sin \delta_i) (I_{ri} - I_{xi}) \quad (2.44)$$

Equation 2.44 gives the complex bus power at i^{th} bus. The next equation shows the bus current components that are derived from Equation 2.44.

$$I_{ri} = \frac{1}{|V_i|} (P_i \cos \delta_i + Q_i \sin \delta_i) \quad (2.45)$$

$$I_{xi} = \frac{1}{|V_i|} (P_i \sin \delta_i - Q_i \cos \delta_i)$$

In the following expression, the final step of the general transmission loss formula derivation is performed by putting the current vectors in Equation 2.45 to Equation 2.43.

$$P_{\text{loss}} = \sum_{i=1}^n \sum_{k=1}^n \alpha_{ik} (P_i P_k + Q_i Q_k) + \beta_{ik} (Q_i P_k - P_i Q_k) \quad (2.46)$$

In Equation 2.46, α and β notations are used for clarity. The real component of the bus impedance matrix (R) is used in Equation 2.47.

$$\alpha_{ik} = \frac{R_{ik}}{|V_i||V_k|} \cos(\delta_i - \delta_k) \quad (2.47)$$

$$\beta_{ik} = \frac{R_{ik}}{|V_i||V_k|} \sin(\delta_i - \delta_k)$$

2.9.2 Incremental Transmission Loss Formula

Incremental transmission loss (ITL) at bus j can be found by taking the partial derivative of power losses (P_L) with respect to generation power (P_G) at that bus.

Suppose that $P_j = P_{Gj} - P_{Dj}$ and P_{Dj} is the demanded power. Replace P_{Gj} with P_j according to this relationship.

$$(\text{ITL})_j = \frac{\partial P_L}{\partial P_{Gj}} = \sum_{i,k=1}^n \frac{\partial}{\partial P_j} [\alpha_{ik}(P_i P_k + Q_i Q_k) + \beta_{ik}(Q_i P_k - P_i Q_k)] \quad (2.48)$$

Partial differentiation terms of Equation 2.48 are shown in Table 2.2 which corresponds to summation indices i and k .

Table 2.2. Partial Differentiation of Equation 2.48

Index		Differentiated Part			
i	k	$\frac{\partial}{\partial P_j} (\alpha_{ik} P_i P_k)$	$\frac{\partial}{\partial P_j} (\alpha_{ik} Q_i Q_k)$	$\frac{\partial}{\partial P_j} (\beta_{ik} Q_i P_k)$	$\frac{\partial}{\partial P_j} (-\beta_{ik} P_i Q_k)$
$i = j$	$k = j$	$2P_j \alpha_{jj}$	0	0	0
$i = j$	$k \neq j$	$P_k \left(\alpha_{jk} + P_j \frac{\partial \alpha_{jk}}{\partial P_j} \right)$	$Q_j Q_k \frac{\partial \alpha_{jk}}{\partial P_j}$	$Q_j P_k \frac{\partial \beta_{jk}}{\partial P_j}$	$-Q_k \left(\beta_{jk} + P_j \frac{\partial \beta_{jk}}{\partial P_j} \right)$
$i \neq j$	$k = j$	$P_i \left(\alpha_{ij} + P_j \frac{\partial \alpha_{ij}}{\partial P_j} \right)$	$Q_i Q_j \frac{\partial \alpha_{ij}}{\partial P_j}$	$Q_i \left(\beta_{ij} + P_j \frac{\partial \beta_{ij}}{\partial P_j} \right)$	$-P_i Q_j \frac{\partial \beta_{ij}}{\partial P_j}$
$i \neq j$	$k \neq j$	$P_i P_k \frac{\partial \alpha_{ik}}{\partial P_j}$	$Q_i Q_k \frac{\partial \alpha_{ik}}{\partial P_j}$	$Q_i P_k \frac{\partial \beta_{ik}}{\partial P_j}$	$-P_i Q_k \frac{\partial \beta_{ik}}{\partial P_j}$

Rewrite ITL Equation 2.48 using Table 2.2:

$$\begin{aligned}
(ITL)_j = & 2P_j\alpha_{jj} + \sum_{\substack{k=1 \\ k \neq j}}^n \left[\alpha_{jk}P_k - \beta_{jk}Q_k + (P_jP_k + Q_jQ_k) \frac{\partial \alpha_{jk}}{\partial P_j} + (Q_jP_k - \right. \\
& \left. P_jQ_k) \frac{\partial \beta_{jk}}{\partial P_j} \right] + \sum_{\substack{i=1 \\ i \neq j}}^n \left[\alpha_{ij}P_i + \beta_{ij}Q_i + (P_iP_j + Q_iQ_j) \frac{\partial \alpha_{ij}}{\partial P_j} + (Q_iP_j - P_iQ_j) \frac{\partial \beta_{ij}}{\partial P_j} \right] + \\
& \sum_{\substack{i=1 \\ i \neq j}}^n \sum_{\substack{k=1 \\ k \neq j}}^n \left[(P_iP_k + Q_iQ_k) \frac{\partial \alpha_{ik}}{\partial P_j} + (Q_iP_k - P_iQ_k) \frac{\partial \beta_{ik}}{\partial P_j} \right] \quad (2.49)
\end{aligned}$$

Note that $\alpha_{ik} = \alpha_{ki}$ and $\beta_{ik} = -\beta_{ki}$. Let us use different representation for longer partial derivative representation:

$$\frac{\partial \alpha_{ik}}{\partial P_j} = \alpha'_{ik} \text{ and } \frac{\partial \beta_{ik}}{\partial P_j} = \beta'_{ik} \quad (2.50)$$

Now, rewrite Equation 2.49 using expressions given in Equation 2.50.

$$(ITL)_j = 2 \sum_{k=1}^n [\alpha_{jk}P_k - \beta_{jk}Q_k] + \sum_{k=1}^n [(P_iP_k + Q_iQ_k)\alpha'_{ik} - (P_iQ_k - Q_iP_k)\beta'_{ik}] \quad (2.51)$$

Then we will derive a different expression for partial derivatives of α and β in Equation 2.51 using the formula shown in Equation 2.46.

$$\frac{\partial \alpha_{ik}}{\partial P_j} = \alpha'_{ik} = -\frac{R_{ik}}{|V_i||V_k|} \sin(\delta_i - \delta_k) \left(\frac{\partial \delta_i}{\partial P_j} - \frac{\partial \delta_k}{\partial P_j} \right) \quad (2.52)$$

$$\frac{\partial \beta_{ik}}{\partial P_j} = \beta'_{ik} = \frac{R_{ik}}{|V_i||V_k|} \cos(\delta_i - \delta_k) \left(\frac{\partial \delta_i}{\partial P_j} - \frac{\partial \delta_k}{\partial P_j} \right)$$

Bus power injection can be found by using Equation 2.10:

$$P_i = \text{Re}\{\sum_{k=1}^n Y_{ik} V_k V_i^*\} \quad (2.53)$$

Equation 2.54 shows the representation of bus voltages and elements of bus admittance matrix in polar form.

$$V_i^* = |V_i| e^{-j\delta_i} \quad (2.54)$$

$$V_k = |V_k| e^{j\delta_k}$$

$$Y_{ik} = |Y_{ik}| e^{j\varphi_{ik}}$$

Rewrite Equation 2.53 using the polar form of bus voltages and bus admittances matrix entries as follows.

$$P_i = \text{Re}\{\sum_{k=1}^n |Y_{ik} V_k V_i| e^{j(\delta_k - \delta_i + \varphi_{ik})}\} \quad (2.55)$$

Real part of injected power (P_i) can be shown as given in Equation 2.56.

$$P_i = \sum_{k=1}^n |Y_{ik} V_k V_i| \cos(\delta_k - \delta_i + \varphi_{ik}) \quad (2.56)$$

Equation 2.57 is obtained by differentiating Equation 2.56.

$$\frac{\partial P_i}{\partial \delta_j} = - \left| |Y_{ij} V_j V_i| \sin(\delta_j - \delta_i + \varphi_{ij}) \right| \quad (2.57)$$

$$\frac{\partial \delta_j}{\partial P_i} = - \frac{1}{\left| |Y_{ij} V_j V_i| \sin(\delta_j - \delta_i + \varphi_{ij}) \right|}$$

Now, substitute Equation 2.57 into Equation 2.52:

$$\alpha'_{ik} = \frac{R_{ik} \sin(\delta_i - \delta_k)}{|V_j| |V_i| |V_k|} \left[\frac{1}{\left| |Y_{ij}| |V_i| \sin(\delta_i - \delta_j + \varphi_{ji}) \right|} - \frac{1}{\left| |Y_{jk}| |V_k| \sin(\delta_k - \delta_j + \varphi_{jk}) \right|} \right] \quad (2.58)$$

$$\beta'_{ik} = \frac{R_{ik} \cos(\delta_i - \delta_k)}{|V_j| |V_i| |V_k|} \left[\frac{1}{\left| |Y_{jk}| |V_k| \sin(\delta_k - \delta_j + \varphi_{jk}) \right|} - \frac{1}{\left| |Y_{ji}| |V_i| \sin(\delta_i - \delta_j + \varphi_{ji}) \right|} \right]$$

After substituting Equation 2.58 into Equation 2.51, it is noticed that the second sum part of Equation 2.51 is negligible, as Elgerd stated in [37]. Hence, incremental transmission loss can be calculated as given in Equation 2.59.

$$(\text{ITL})_j = \frac{\partial P_L}{\partial P_j} \approx 2 \sum_{k=1}^n [\alpha_{jk} P_k - \beta_{jk} Q_k] \quad (2.59)$$

The foundation of the loss sensitivity factor (LSF) is based on Equation 2.59. This is because LSF indicates the amount of change in losses due to the variation of bus injection power at that bus. Hence, ITL expression can be directly replaced with LSF.

CHAPTER 3

PROBLEM FORMULATION AND METHODOLOGY

This chapter describes the two-problem related to BESS application and explains the methods to be applied to solve these problems that are defined as follows:

- i) Given the MW capacity of the battery, finding the optimum location to be placed in terms of reducing grid losses.
- ii) Given the location of the battery, implementing a cost-benefit analysis by calculating the BESS investment cost and savings obtained from electrical energy trading for different sizes of BESS.

In the first section, finding the optimum location problem for BESS application is presented. A LSF based method, named as Δ LSF calculation, is preferred to determine the best BESS location considering losses. The following section explains the cost-benefit analysis to decide the storage system size. This analysis is based on covering the cost of operation and investment utilizing the savings obtained from electrical energy trading and reduced losses due to BESS operation.

3.1 Optimum BESS Placement

Finding optimum BESS location is one of the most critical concern for energy storage investments. Improper placement can disturb the reliability and stability of the system. These disturbances appear because BESSs can act as both load and generation. Literature research shows the prevailing method for finding optimum BESS location is Δ LSF calculation. LSF method is based on incremental transmission loss, which is explained in Chapter 2. The logic of the LSF calculation is presented in this section.

In Equations 3.1 and 3.3, active power loss ($P_{L,t}$) and incremental loss formulations are converted to hourly-based forms by reorganizing Equation 2.59 and Equation 2.46. Note that the incremental loss formula given in Equation 2.59 is directly used for the LSF calculation and naming changed from ITL to LSF on the left side of the equation.

$$P_{L,t} = \sum_{i=1}^n \sum_{j=1}^n [\alpha_{ij}(P_{i,t}P_{j,t} + Q_{i,t}Q_{j,t}) + \beta_{ij}(Q_{i,t}P_{j,t} - P_{i,t}Q_{j,t})] \quad (3.1)$$

Equation 3.2 defines the daily power losses of the system on an hourly basis.

$$D_L = \sum_{t=1}^{24} P_{L,t} \quad (3.2)$$

$$(\text{LSF}_{i,t}) = \frac{\partial P_{L,t}}{\partial P_{i,t}} \approx 2 \sum_{j=1}^n [\alpha_{ij}P_{j,t} - \beta_{ij}Q_{j,t}] \quad (3.3)$$

In Equations 3.1 to 3.4, $P_{i,t}$ is active power injection, $V_{i,t}$ is bus voltage, $\delta_{i,t}$ is bus voltage angle, at time t . Real component of the ij^{th} element of the bus impedance matrix is denoted by r_{ij} . Previously defined α and β terms are also converted to time-based types in Equation 3.4.

$$\alpha_{ij} = \frac{r_{ij}}{|V_{i,t}||V_{j,t}|} \cos(\delta_{i,t} - \delta_{j,t}) \quad (3.4)$$

$$\beta_{ik} = \frac{r_{ij}}{|V_{i,t}||V_{j,t}|} \sin(\delta_{i,t} - \delta_{j,t})$$

The relationship between incremental transmission loss and loss sensitivity factor is explained as follows. Equation 3.3 specifies the amount of change in losses due to active power variation at the relevant bus [18]. In the literature, this is called as the loss sensitivity of the related bus and hence the method is named as Loss Sensitivity Factor. LSF can also be calculated based on reactive power. However, the power factor of BESS is assumed to be unity.

As described in Chapter 1, several studies have been published related to the LSF method. This method is commonly implemented for capacitor bank placements. In recent years, this method has been adopted to the determination of the optimal BESS location. However, in the vast majority of articles, it is recommended to place BESS at the buses that have minimum LSF. This is because BESSs are considered to behave in the same way as capacitor banks. For this reason, these methods disregard the fact that the BESS has two modes of operation, charging and discharging. Choosing the bus, which gives minimum LSF means that the battery only works in discharge mode. This idea is put forward because it is reasonable to choose the bus which affects the losses the least. In order to overcome this missing perspective, the scenario where the battery is charged, in other words, it works as a load, should also be considered.

After emphasizing that the battery should be handled in both modes of operation, it is necessary to correlate this event with the daily load curve. In this thesis, it is assumed that the battery is charged once and discharged once a day. As mentioned in Chapter 2, electrical energy prices vary during the day thanks to the time-of-use tariff, or spot pricing. In the presented method, it is considered that the battery is charged when the energy prices are low, then it is discharged to support the grid when the electricity prices are high. Hence, the difference between peak and lowest prices must be as high as possible.

Let us examine Turkey's intraday country market electricity prices on 29.07.2019, as shown in Figure 3.1. In Figure 3.1, it can be seen that the prices reached their peak between 15:00 and 18:00. On that day, after midnight hours, between 03:00 and

06:00, the market prices hit bottom. Obviously, it will be a profitable choice to charge the battery during hours after midnight and discharge it during late afternoon hours. As it can be observed from Figure 3.1, there is no guarantee that the prices will be high in the neighboring hours of the peak price hour. The same observation is valid for the case situation that prices hit bottom. For this reason, a certain time interval is determined when choosing the hours to be charged or discharged. The average of the prices in these selected hour intervals is taken. The hour interval with the highest average determines the hours to be discharged. On the other hand, the hour interval with the lowest average indicates the hours to be charged. Charging and discharging intervals are illustrated in Figure 3.2.

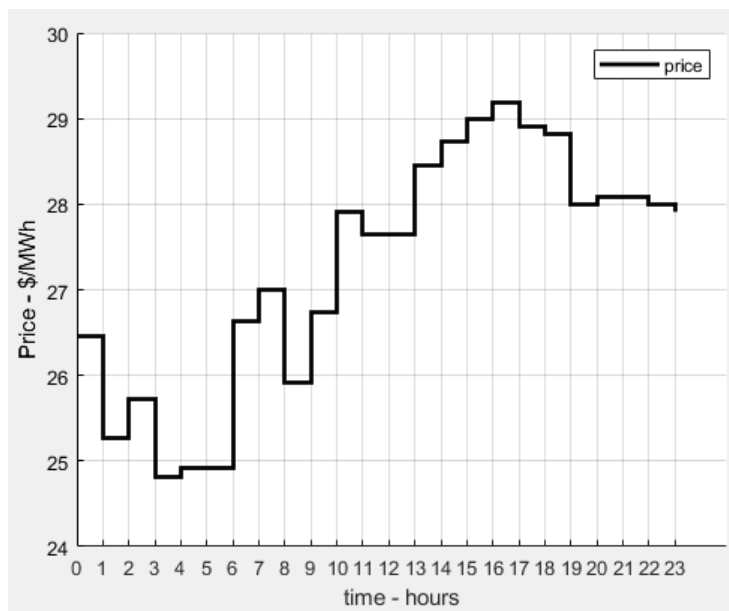


Figure 3.1. Intraday Market Energy Prices on 29.07.2019, Source: Energy Exchange Istanbul [23]

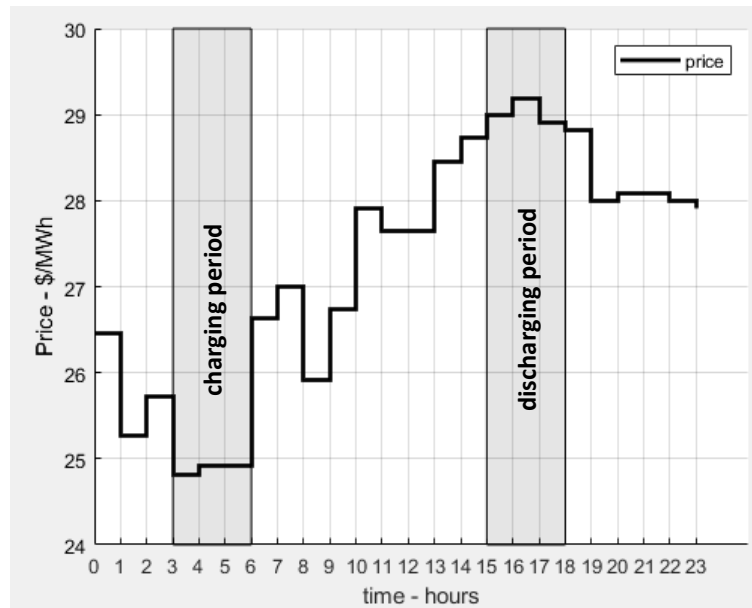


Figure 3.2. Charging and Discharging Periods on Intraday Market Energy Prices Curve

The daily load curve and daily energy price curve are combined in Figure 3.3. In this figure, it can be seen that load demand is almost at the lowest level in the charging interval. On the other hand, system load is considerably high in the discharging period. In this way, it is seen that the proposed method also contributes to the peak shaving process which is described elaborately in Chapter 2. In this way, it is confirmed that the applied method also contributes to the peak shaving process which is described in detail in Chapter 2.

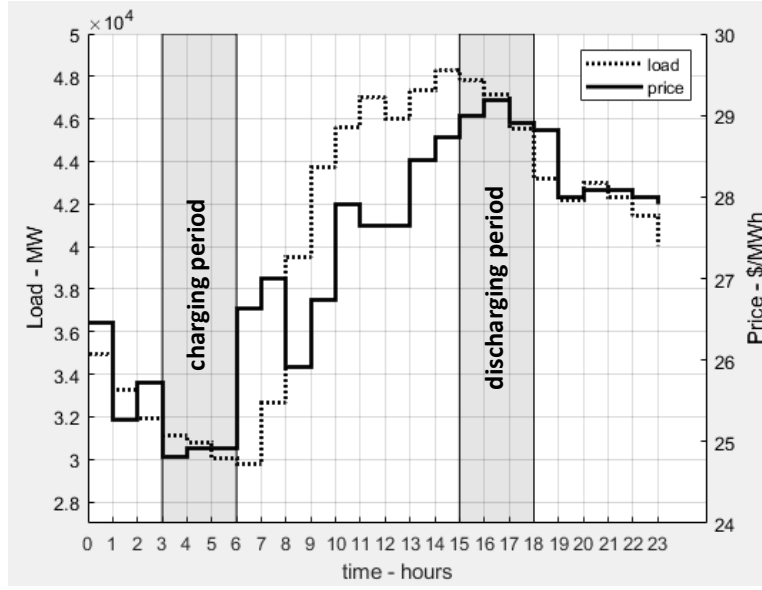


Figure 3.3. Combination of Daily Load and Daily Energy Price Curves

When Equation 3.3 is examined, it is seen that LSF is calculated at a certain instant from power injection and bus voltages. In most studies, this single-shot LSF solution is calculated at peak load conditions. In this thesis, computation of LSF will be made to include the dynamics during the day. Equation 3.5 below is introduced to cover daily changes in the load demand.

$$\Delta \text{LSF} = \text{LSF}_{\text{average}}^{\text{charging}} - \text{LSF}_{\text{average}}^{\text{discharging}} \quad (3.5)$$

where,

$$\text{LSF}_{\text{average}}^{\text{charging}} = \left(\sum_{t=t_{1,ch}}^{t_{ch}} \text{LSF}_t^{\text{charging}} \right) / c \quad (3.6)$$

$$\text{LSF}_{\text{average}}^{\text{discharging}} = \left(\sum_{t=t_{1,dch}}^{t_{dch}} \text{LSF}_t^{\text{discharging}} \right) / c$$

t = Battery Charging/Discharging Hours

$t_{1, \text{ch}}, t_{1, \text{dch}}$ = Charging or Discharging Start Time

$t_{\text{ch}}, t_{\text{dch}}$ = Charging or Discharging End Time

c = Total Charging/Discharging Duration in Hours

Discharging BESS during the peak load demand period, which is located on a bus with lower LSF, should raise the loss reduction. On the other hand, charging BESS during the low load demand, which is located on a bus with higher LSF, should decrease grid losses increment. Choosing a bus with the highest ΔLSF gives the optimal bus location where BESS should be placed. In the continuation of the thesis, the optimal BESS positioning method will be called ΔLSF .

When Equation 3.5 is examined, it is noticed that LSF is calculated for each hour of the day. At the end of this process, twenty-four different hourly LSF values are obtained for a bus. As expected, this daily LSF calculation process is repeated for other buses as well. Eventually, hourly LSF calculation data are obtained for all buses. In this study, these data are used to create a daily loss sensitivity factor curve. The daily loss sensitivity factor curve will be used to evaluate the optimal BESS location process.

As described in Chapter 2, seasonal variations will also be considered for the representative daily load curve of the year in the testing process. The dates of the daily load curve will be selected as spring minimum, summer peak, and winter peak. Then, daily energy market prices data will be collected from the specified time intervals. It is aimed to find an optimum solution by taking the arithmetic average of the data extracted for three seasons. Arithmetic averages of weekly data are computed to prevent over-design and under-design. Hence, the arithmetic average operation will be applied for daily load and daily electrical energy market price curves.

3.2 Cost-Benefit Analysis for Determination of BESS Sizing

After figuring out where the BESS will be placed, it is also important to determine the size of the battery. As expected, it would be desired to put a battery that provides the highest output power considering the bus and transmission line capacity. Undoubtedly, choosing the maximum will be an easy choice. However, there are financial and production limiting factors other than the physical maximums of the system. The size of the battery is determined by taking into consideration these factors.

As mentioned in Chapter 1, the study proposes several costing parameters to estimate BESS investment realistically [19]. Rated power output and capacity are used to price the battery.

The following terms are used for BESS costing:

EC = Energy Capacity Cost - \$/MWh

PC = Power Conversion Cost - \$/MW

BOP = Balance of Plant Cost - \$/MW

CC = Construction Cost - \$/MWh

OMC = Operation and Maintenance Cost - \$/MW-Year

RE = Round-Trip Efficiency of BESS – Efficiency / 100

DOD = BESS's Depth of Discharge – Charge Depth Percentage / 100

FL = Floating Life of BESS - Years

TDCD = Time Duration of Charge/Discharge - Hours

Energy Capacity Cost (EC) includes BESSs electrodes, electrolytes and similar components. The value of this term can vary greatly depending on the type of electrochemical battery.

A conversion system should be placed since BESS outputs DC power and the grid works with AC. This conversion system is valued by the power conversion cost (PC). Although this value is slightly less for Li-ion batteries, it is the same or close for all types of battery systems.

Balance of Plant Cost (BOP) can be summarized as the connections of the batteries in the field and auxiliary expenses in the substation. This cost is also approximately the same for all other chemical battery types.

Construction Cost (CC) cost is explained as the cost related to the procurance of field equipment, the construction of the field, and the necessary permits to be obtained.

Operation and Maintenance Cost (OMC) is the sum of the required maintenance and expenses for the battery system to work correctly and without failures. In general, it is given as a yearly cost.

After the batteries are charged from the grid, they store energy through electrochemical reactions. In case of discharge, there will be a slight loss while discharging the stored energy back to the system. This loss is taken into consideration by using the Round-Trip Efficiency (RE). RE is assumed as 0.95 in the scope of this thesis work [20].

Time Duration of Charge/Discharge (TDCD) indicates how many hours the battery will be charged or discharged. In this study, the charging and discharging hours will be taken as equal.

Floating Life (FL) is defined as the shelf life of the battery, which is independent of the depth of charge, charge/discharge cycle. This is because batteries are electrochemical equipment and have a life even if they are not used.

Batteries naturally lose their capacity when the charge and discharge cycle advances. The association between this cycle and the depth of the discharge (DOD) of the battery is shown in Figure 3.4. As it can be seen in Figure 3.4, the capacity decreases significantly as the charging cycle increases.

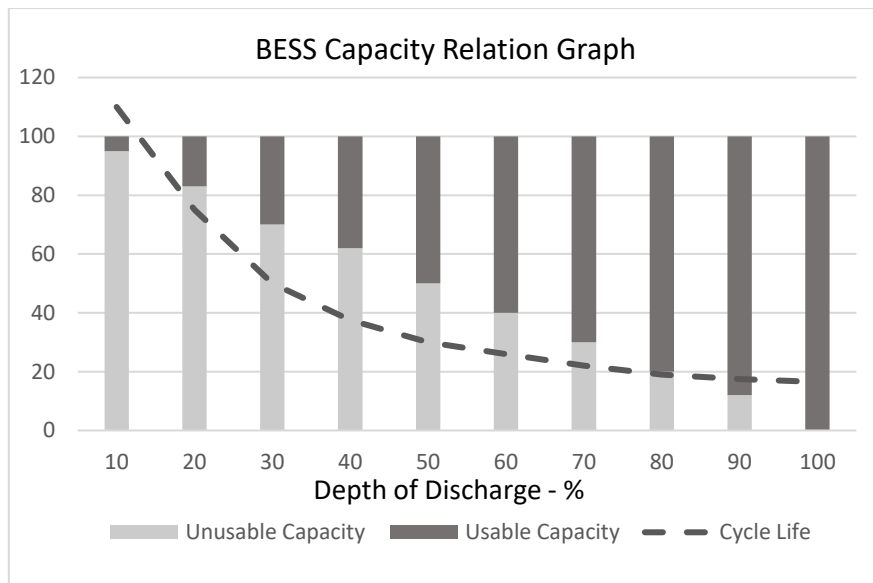


Figure 3.4. The Relationship Between BESS Capacity and Discharging Cycle [21]

On the other hand, many different types of electrochemical batteries are used for energy storage. The correlation between the charging cycle and the depth of discharge of various types of batteries are also different. This relationship is shown in Table 3.1.

As it can be observed from Table 3.1, Li-ion and NaS type batteries are a better choice in terms of capacity loss during high number of cycles comparing the other two types of batteries. Depth of discharge (DOD) is selected by examining Figure 3.4 and Table 3.1. Along with technological developments, there are also improvements in battery technologies. Thanks to these developments, battery production costs are also reduced. The cost reduction for different types of batteries is shown in Table 3.2 with annualized cost reduction percentage.

Table 3.1. BESS Discharging Cycles and Corresponding Capacity Depths [20]

DOD - %	Number of Cycles			
	Lead-Acid	Li-ion	NaS	Ni-Cd
10	8000	-	100000	7900
20	2500	-	60000	5800
30	1500	-	30000	3400
40	950	-	15000	2000
50	700	8000	10000	1200
55	-	7500	-	-
60	590	6900	9000	900
65	-	6200	-	-
70	500	5800	7000	800
75	-	5000	-	-
80	450	4500	6000	700
85	-	4100	-	-
90	390	3700	5000	600
100	350	3000	4000	500

Table 3.2. Cost Reduction Rate of Batteries [20]

Battery type	Annual Cost Reduction Ratio - %
Lead-acid	4.6
Li-ion	5.5
NaS	2.2
NiCd	3

In Table 3.3, BESS pricing parameters for the year 2018 and projections for 2022 are presented. Price projections for the year 2022 is calculated considering cost reduction rate for the Li-Ion battery. The cost-benefit analysis is performed by considering the price decrease over the years, similar to Table 3.3.

Table 3.3. Typical Pricing of BESSs Projected to Year 2022 [19]

cost names \ years	Battery Types					
	Li-ion		Lead-acid		NaS	
	2018	2022	2018	2022	2018	2022
Energy Capacity Cost - \$/kWh	271	216	260	215	661	604
Power Conversion Cost - \$/kW	288	229	350	289	350	320
Balance of Plant Cost - \$/kW	100	79	100	82	100	91
Construction Cost - \$/kWh	101	80	176	145	133	121
Operation & Maintenance Cost - \$/kW-year	10	9	10	9	10	9
Float Life - years	10	10	2.6	2.8	13.5	13.5

$$\text{NET RETURN} = \text{EAC} + \text{LRC} - \text{IOC} \quad (3.7)$$

where,

IOC = Investment and Operation Cost - \$

EAC = Energy Arbitrage Cost - \$

LRC = Loss Reduction Cost - \$

$$\text{IOC} = P^B(\text{PC} + \text{BOP} + \sum_{\text{year}}^{\text{FL}} \text{OMC}) + E^B(\text{EC} + \text{CC}) \quad (3.8)$$

$$\text{EAC} = \sum_{\text{day}}^{\text{FL} \times 360} \left(\sum_{t=t_1, \text{dch}}^{\text{TDCD}} P_t^{\text{disch}} \times C_t \times t - \sum_{t=t_1, \text{ch}}^{\text{TDCD}} P_t^{\text{ch}} \times C_t \times t \right) \quad (3.9)$$

$$\text{LRC} = \sum_{\text{day}}^{\text{FL} \times 360} \left(\sum_{t=t_1, \text{dch}}^{\text{TDCD}} L_t^{\text{disch}} \times C_t \times t - \sum_{t=t_1, \text{ch}}^{\text{TDCD}} L_t^{\text{ch}} \times C_t \times t \right) \quad (3.10)$$

$$E^B = \frac{P^B \times \text{TDCD}}{RE \times \text{DOD}} \quad (3.11)$$

where,

P^B = Rated Power of BESS - MW

E^B = Capacity of BESS – MWh

C_t = Energy Prices at that Hour - \$/MWh

t = Charging/Discharging Duration - Hours

$P_t^{\text{disch}}, P_t^{\text{ch}}$ = Discharging/Charging Power of BESS - MW

$L_t^{\text{disch}}, L_t^{\text{ch}}$ = Loss Reduction During Discharging/Increased Losses During Charging - MW

Net Return in Equation 3.7 refers to the sum of all expenses and savings acquired by implementing the BESS application. This term will be used to evaluate the cost-benefit analysis, and it indicates the breakeven point for BESS investment and savings obtained from BESS usage. The Investment and Operation Cost (IOC) stated in Equations 3.7 and 3.8, includes battery capacity, output power, required physical infrastructures, and operating costs. Energy capacity, power conversion, construction, and balance of plant costs are calculated at the beginning of the analysis, whereas operation and maintenance costs should be calculated annually over a lifetime. Energy Arbitrage Cost (EAC) is used to calculate the savings obtained from electrical energy price differences by trading, and it is calculated by using Equation 3.9. In Equation 3.10, Loss Reduction Cost (LRC) is given to assess the reduced grid losses due to the locating BESS to the system. L_t^{disch} and L_t^{ch} can be achieved by finding difference between grid losses with and without BESS. Capacity of

BESS (E^B) is found from energy capacity cost, power conversion cost, round-trip efficiency cost, and depth of discharge as given in Equation 3.11.

In Chapter 3, at first, the methodology that will be utilized for finding optimum BESS placement has been explained. The application procedure of the Δ LSF method has been described. Secondly, the cost-benefit analysis has been proposed to determine BESS size considering electrical energy trading. In this analysis, it is assumed that the net return of the battery storage system investment will be assessed considering energy trading via BESS. In the following chapter, the presented method for optimum BESS placement and the cost-benefit analysis related to BESS sizing will be evaluated under various conditions and power systems.

CHAPTER 4

TESTS AND EVALUATIONS

After explaining the methods to be applied and the technical background to be used, the proposed approach will be applied to various test systems. First, the determination of daily load and electrical energy market prices curves are described. Next, the optimal placement of BESS will be validated for different output power ratings of BESS. Three different power grids are chosen for testing simulations, IEEE 14-Bus, 9-Bus, and IEEE 33-Bus. Last, the cost-benefit analysis for sizing of BESS will be evaluated. The analysis will be done using BESS power ratings that are tested for optimal placement battery.

4.1 Optimal Placement of BESSs

Optimum positioning of battery energy storage systems is validated with the Δ LSF method. The approach based on Δ LSF, which was explained in Chapter 3, will be implemented on the following three test systems.

- i) Test System-I: IEEE 14-Bus [38]
- ii) Test System-II: 9-Bus [39]
- iii) Test System-III: IEEE 33-Bus [40]

Test System-I contains 14 buses, 5 generators, and 11 loads. Note that the total load demand is 259.00 MW, and the total generation is 272.39 MW for the test case. Test System-II has 9 buses, 3 generators, and 3 loads. The total load demand is 315.00 MW, and the total generation is 319.64 MW for the second test case. Test System-III contains 33 buses, a generator, and 32 loads. The total generation of this generator is 3.92 MW, and the total system load demand is 3.72 MW. The single-line diagrams of the test systems are shown in Figure 4.1, Figure 4.2, and Figure 4.3, respectively.

The test systems' bus, generator, and branch data are given in Appendices A, B, and C. Δ LSF calculations are implemented on MATLAB environment [43] using MATPOWER tool [42]. Equation 3.3 and Equation 3.4 are used to find the average LSF values given in Equation 3.5.

To implement Equation 3.4, the bus impedance matrix of the investigated test system must be created. The construction of the bus admittance matrix is described in Section 2.7.1. Bus admittance matrix in this study is created by using MATPOWER tool. The bus impedance matrix is found by taking the inverse of the bus admittance matrix. Bus voltages and angles, which are other variables required to implement Equation 3.4, are found using MATPOWER with the AC power flow method. When Equation 3.5 is examined, power injections in the system should be known for battery positioning. These power injections are also taken from power flow analysis implemented on MATLAB.

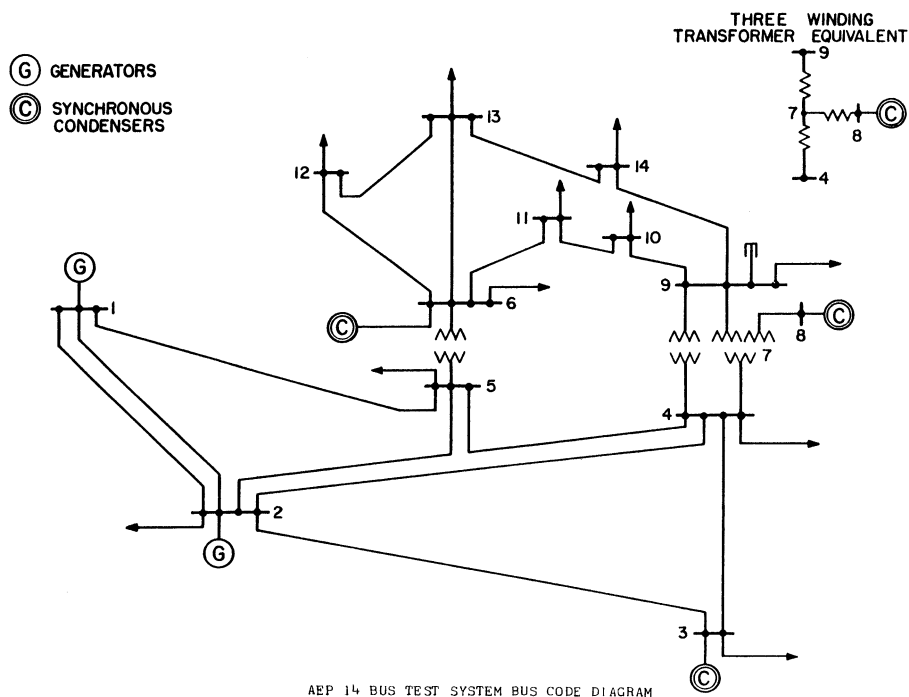


Figure 4.1. IEEE 14-Bus Test Case Single Line Diagram [38]

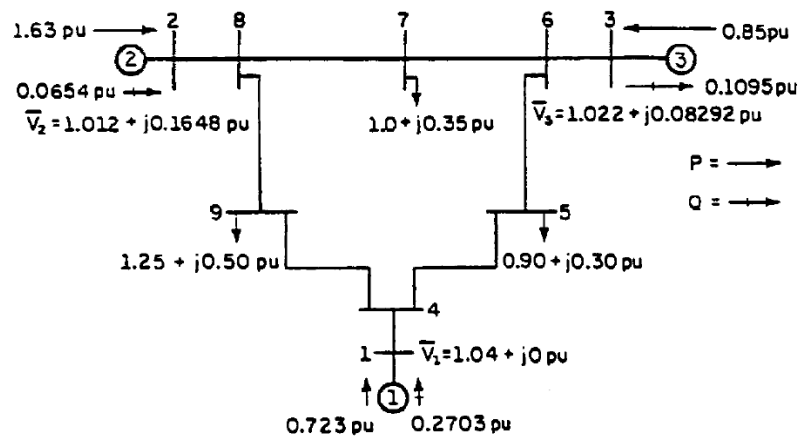


Figure 4.2. 9-Bus Test Case Single Line Diagram [39]

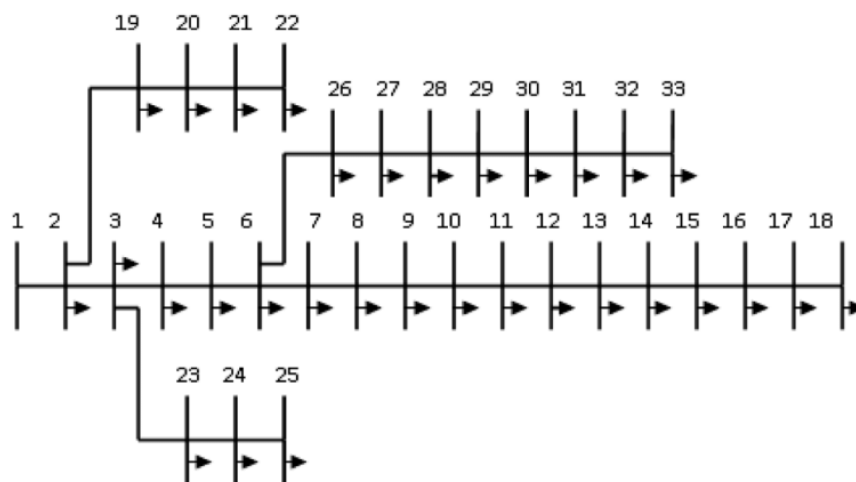


Figure 4.3. IEEE 33-Bus Test Case Single Line Diagram [40]

4.1.1 Determining Daily Load Curve and Electrical Energy Pricing

Turkish electricity system data provided by Energy Exchange Istanbul (EXIST) [23] are used for obtaining the daily load and electricity market prices curves. Publicly available data provided by EXIST can be accessed via the website. Our purpose is to find synthetic daily load and electrical energy market prices curves and the data extracted from EXIST serve for this purpose. Data snapshots were taken at three

different weeks of the year to consider seasonal differences in load demand. The dates of data collection are given as follows:

- 23.03.2020 - 29.03.2020
- 06.07.2020 - 12.07.2020
- 10.12.2020 - 16.12.2020

Data snapshots are provided on an hourly basis. In order to observe the weekly load demand change, 168 hours of data are captured, which corresponds to one week. The data between 23.03.2020 and 29.03.2020 are used for the spring minimum conditions. The dates between 06.07.2020 - 12.07.2020 are selected for the summer peak load condition. Finally, the period between 10.12.2020 and 16.12.2020 is used to observe the winter conditions. Seasonal load demands are shown in Figure 4.4, Figure 4.5, and Figure 4.6. Figure 4.7 is obtained by taking the arithmetic average of these figures.

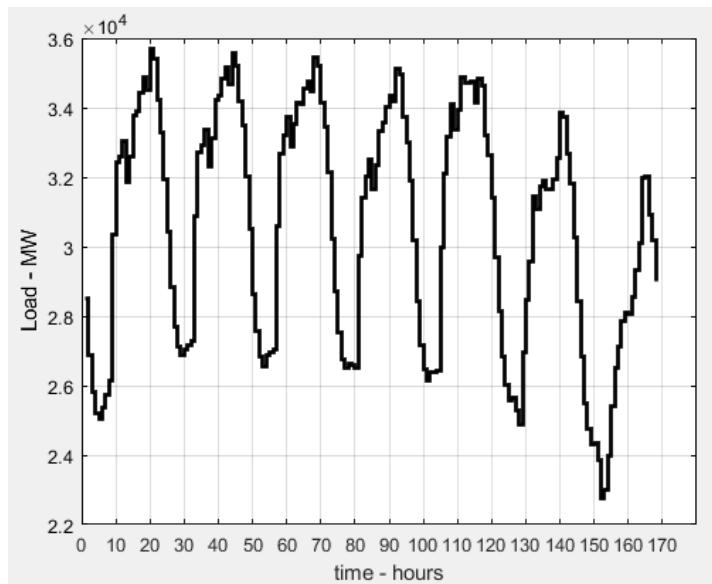


Figure 4.4. Daily Load Curve Based on Country Load of Turkey, Spring Minimum,
Date: 23.03.2020-29.03.2020 [23]

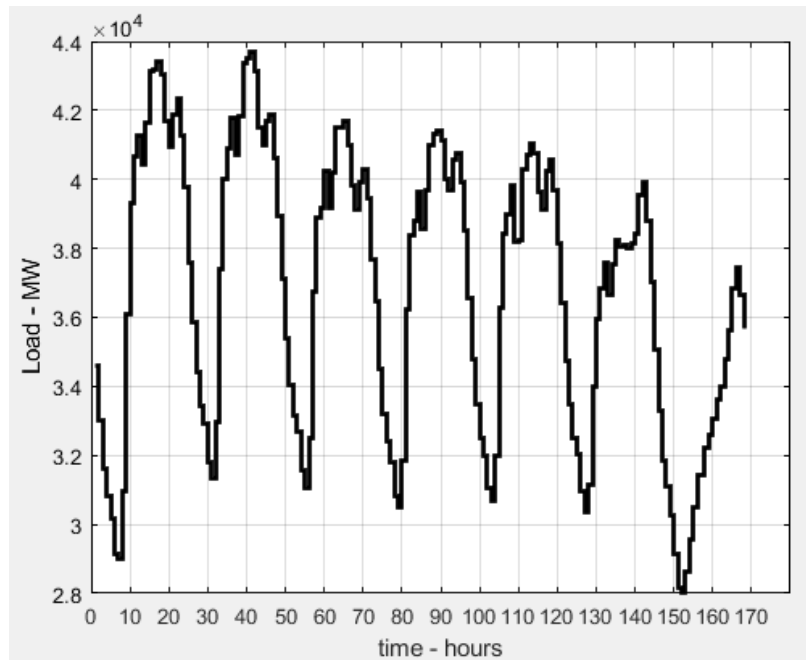


Figure 4.5. Daily Load Curve Based on Country Load of Turkey, Summer Peak, Date: 06.07.2020-12.07.2020 [23]

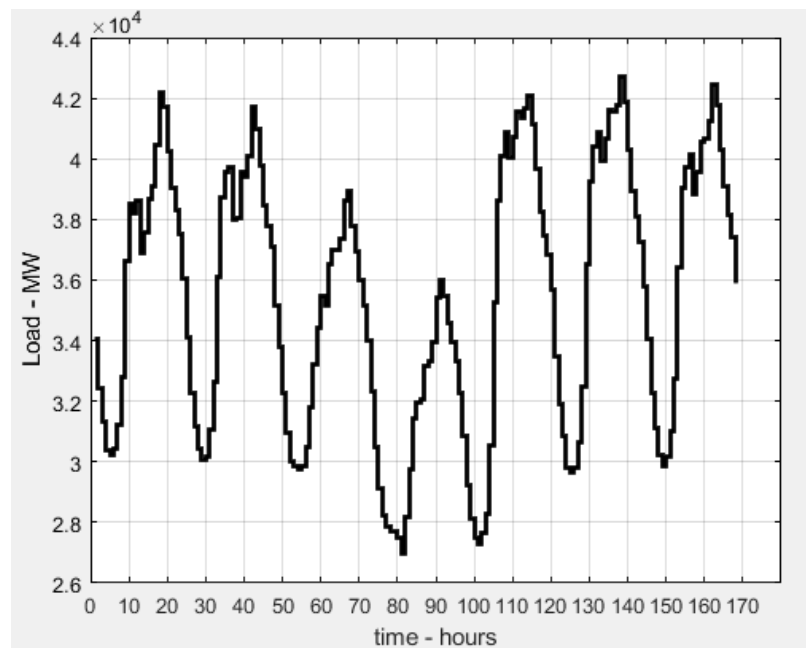


Figure 4.6. Daily Load Curve Based on Country Load of Turkey, Winter, Date: 10.12.2020-16.12.2020 [23]

As it can be seen from Figure 4.7, the load demand decreases on weekends. In addition, while the load demand is minimum in the midnight, it reaches maximum levels in the evening hours as expected. Note that these expectations are valid for the given daily country load demand which is a combination of various types of consumer profiles.

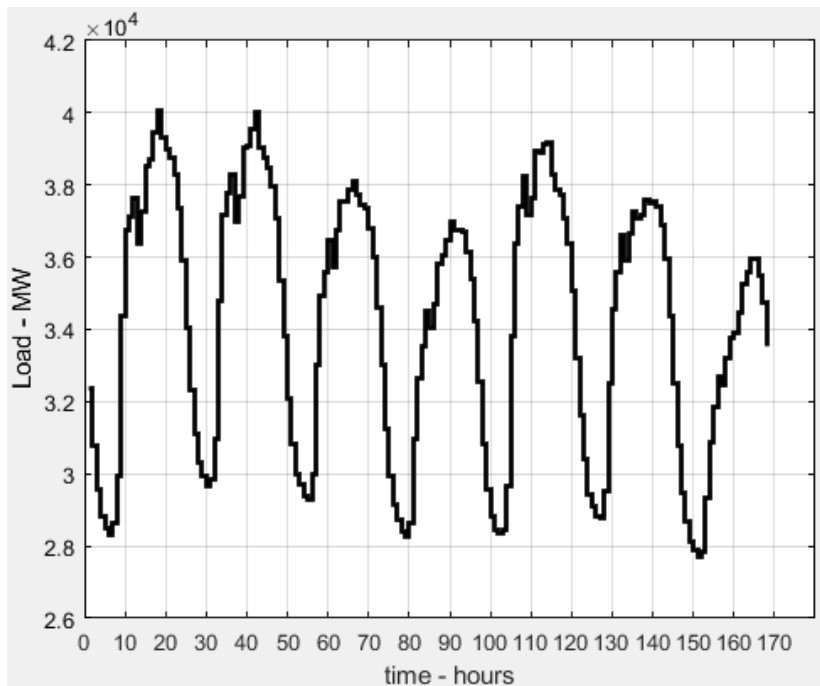


Figure 4.7. Daily Load Curve Obtained by Averaging Three Seasonal Data

Intraday energy prices showing seasonal differences are given in Figure 4.8, Figure 4.9, and Figure 4.10. Data received from Energy Exchange Istanbul is in Turkish Lira. In this study, US dollars is chosen as the currency. In order to be consistent, all prices are converted to US dollars. US Dollars to Turkish Lira conversion is made at the rate of 1 USD equals 11 Turkish Liras.

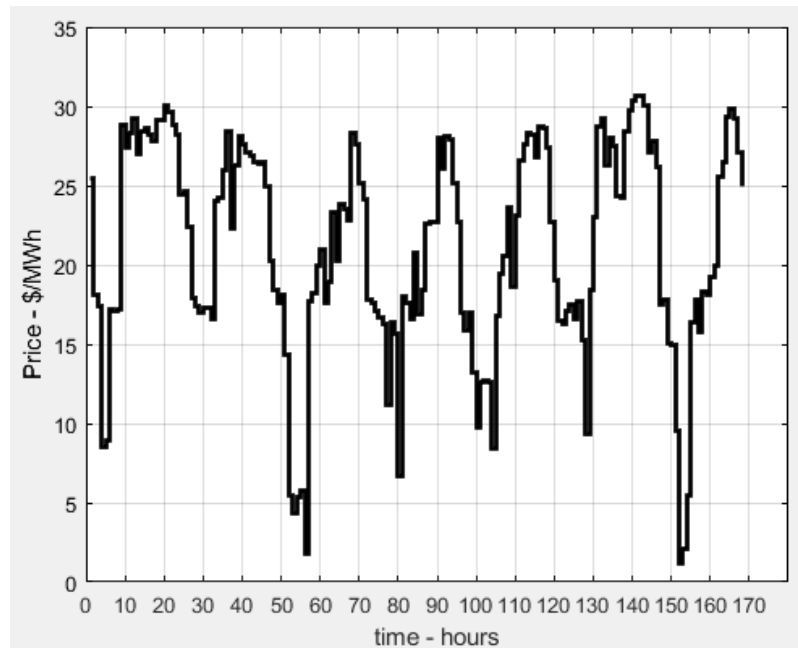


Figure 4.8. Intraday Country Electrical Energy Prices of Turkey, Spring Minimum,
Date: 23.03.2020-29.03.2020 [23]

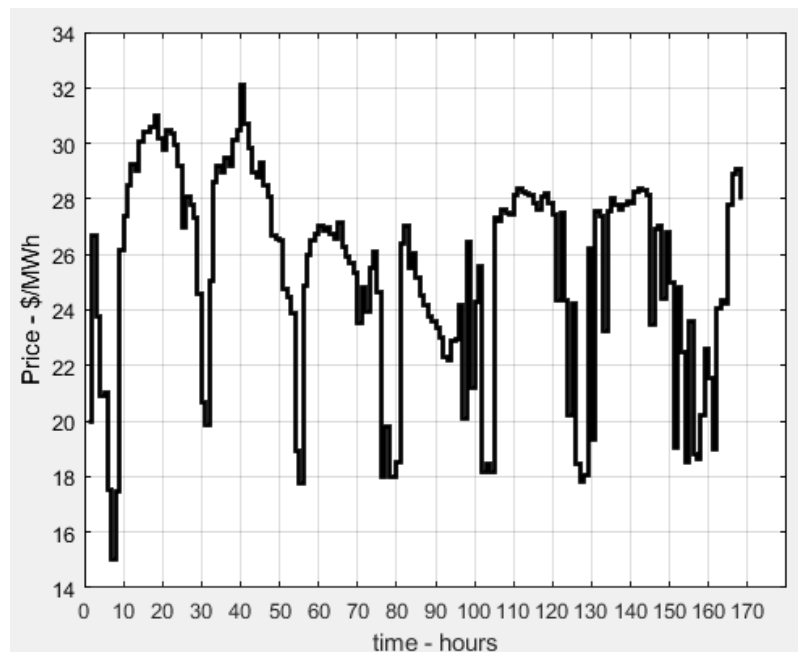


Figure 4.9. Intraday Country Electrical Energy Prices of Turkey, Summer Peak,
Date: 06.07.2020-12.07.2020 [23]

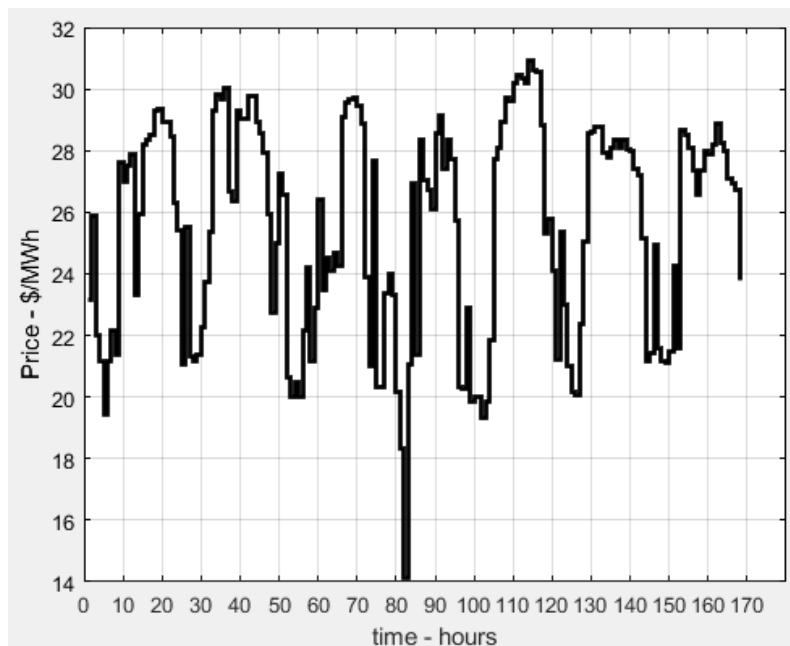


Figure 4.10. Intraday Country Electrical Energy Prices of Turkey, Winter, Date: 10.12.2020-16.12.2020 [23]

As it can be seen in Figure 4.11, a single chart is obtained for the electrical energy prices curve by taking the arithmetic average of seasonal electricity prices. Energy market prices vary similarly to the daily load demand due to the free-market economy and market competition.

Figures obtained so far related to daily load and electrical energy market prices curves contain weekly data. It is observed that the market prices and load demand show different characteristics for each day in a week. Since our strategy is an approximate approach, arithmetic averages of weekly data are computed to prevent over-design and under-design. In Figure 4.12, the 24-hours average daily load demand graph is obtained by taking the arithmetic average of each hour using the previous data, which are given as weekly. In other words, 24-hours data is created using 1-week data. An intraday electrical energy price curve is created using the same procedure, as shown in Figure 4.13.

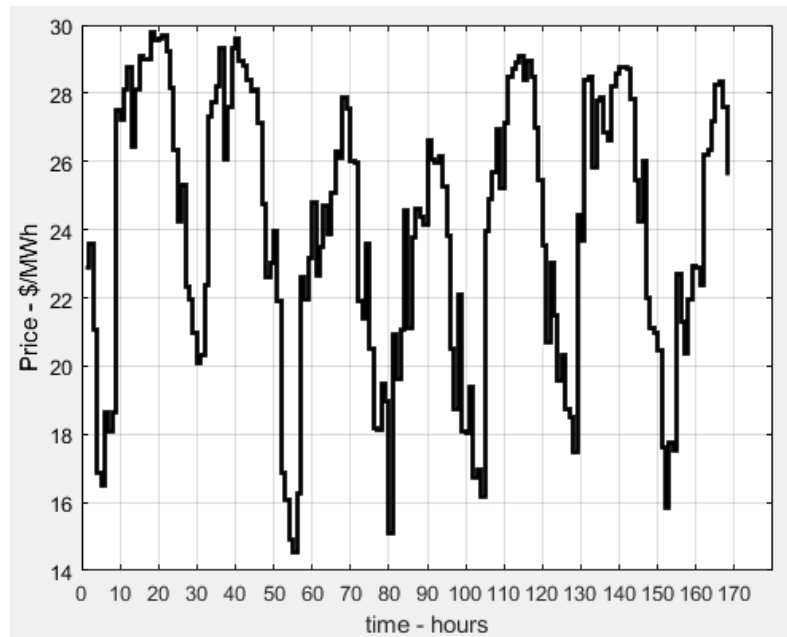


Figure 4.11. Intraday Electrical Energy Prices of Turkey Obtained by Averaging Three Seasonal Data

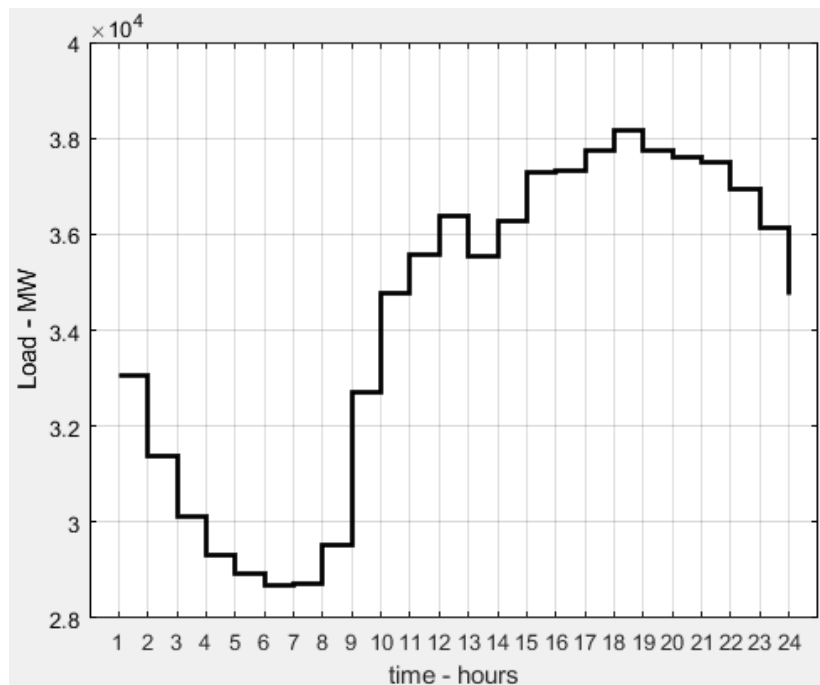


Figure 4.12. 24-Hours Daily Load Curve Obtained by Averaging Weekly Data

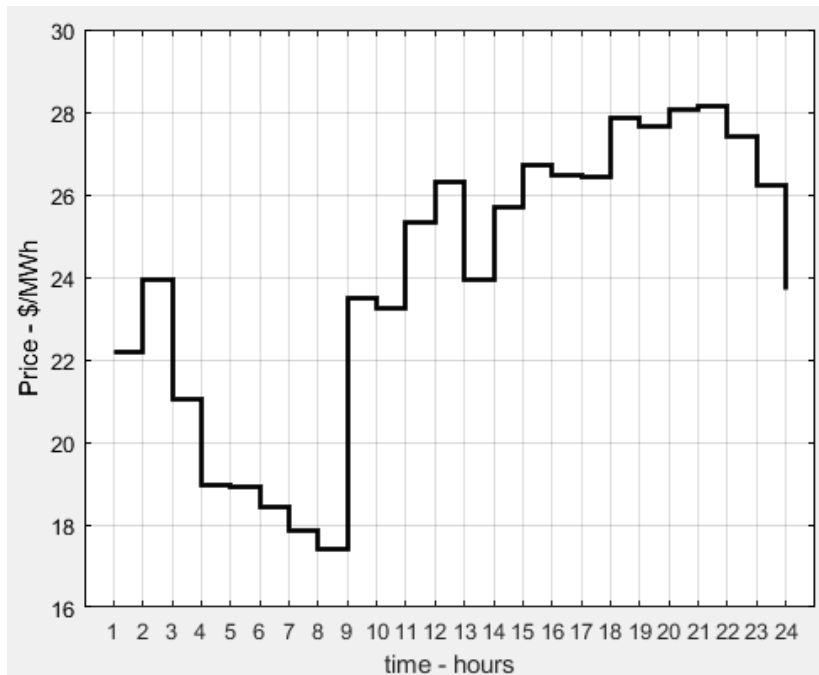


Figure 4.13. 24-Hours Electrical Energy Prices Curve Obtained by Averaging Weekly Data

It is expected that there will be parallelism between daily load demand and energy prices. Figure 4.14 illustrates this relationship by combining the daily load curve with the intraday electrical energy prices graphs. When Figure 4.14 is examined, the volatility of daily demand is followed by the electrical energy prices curve.

The charging and discharging times of the battery are determined according to the prices. In Figure 4.14, the first shaded area shows the charging hours of the BESS, and the second shaded area exhibits the discharging hours. According to the methodology, the average prices of the 3-hours windows are calculated during a day. These windows are compared to each other to specify the charging and discharging hours, which yields maximum savings. The window width is chosen as three hours considering the durations of charging and discharging.

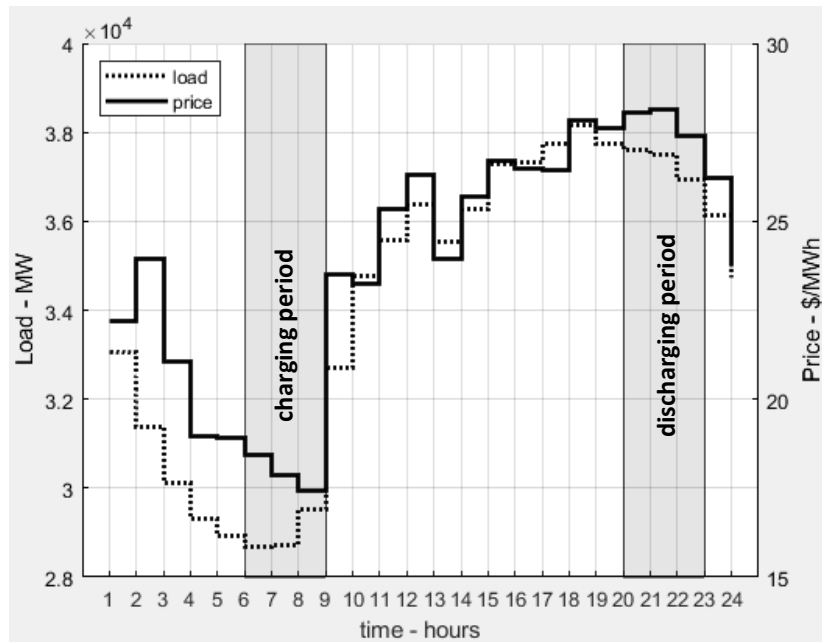


Figure 4.14. Combination of 24-Hours Electrical Energy Prices and Daily Load Curves

4.1.2 Calculation of Loss Sensitivity Factors

Loss sensitivity factor calculation is performed using Equation 3.3. AC power flow analysis is conducted for each LSF calculation. First, LSFs are calculated for each hour according to the hourly load given in Figure 4.12. Then, after finding LSF values for a bus during a day, the calculation process continues separately for other buses. The obtained LSF values for all buses are presented in a curve, namely daily LSF. Next, Δ LSFs are calculated using Equation 3.5 and daily LSF data. Simulations are implemented on three test systems. Since the Δ LSF method proposes a BESS location that reduces grid losses as much as possible, validation of this method is presented by comparing grid losses during the operation of BESS. In this study, BESS is in operation for three hours during the charging and discharging process, as stated before. Hence, grid losses are calculated for six hours to verify optimum BESS location results.

4.1.2.1 Test System-I: 14-Bus Case

In Test System-I, the IEEE 14-Bus test case will be examined to validate the Δ LSF method. The total load demand of the IEEE 14-Bus case is 259.00 MW, and this value is assumed to be the maximum load in the daily load curve. Also, load demands are scaled accordingly for the remaining hours.

Daily LSF calculation on Test System-I is given in Figure 4.15. As expected, the LSF value of a bus varies during the day due to the daily load curve. The Δ LSF calculation is shown in Figure 4.16 for this system. According to the results, it is observed that positioning the battery at Bus-3 or Bus-14 would be a logical choice since Δ LSF values of these buses are higher than the others. The reason for choosing two different buses is that the two values are remarkably close to each other. The difference between Δ LSF for Bus-3 and Δ LSF for Bus-14 is only 1.3 percent. The bus with the largest Δ LSF calculation is searched according to the presented methodology. As a result, two different BESS locations will be investigated for the validation, which are Bus-3 and Bus-14.

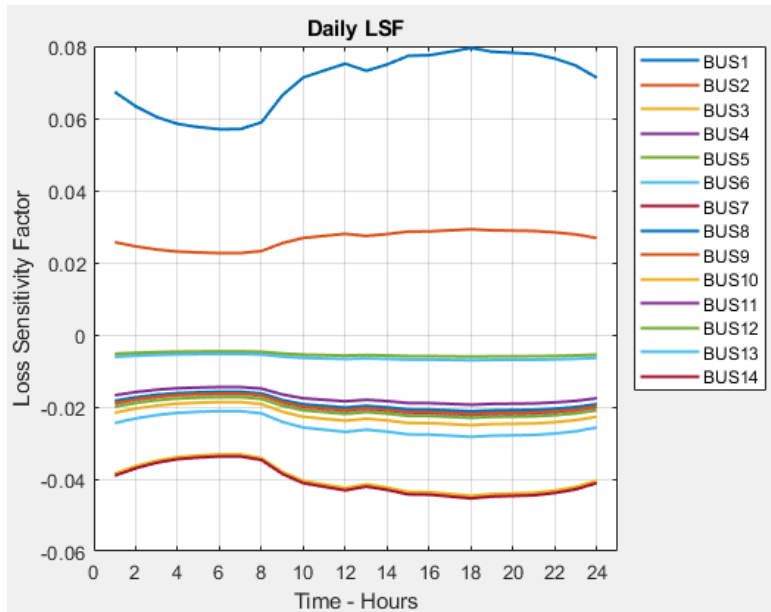


Figure 4.15. Daily LSF Calculation for 14-Bus Test Case

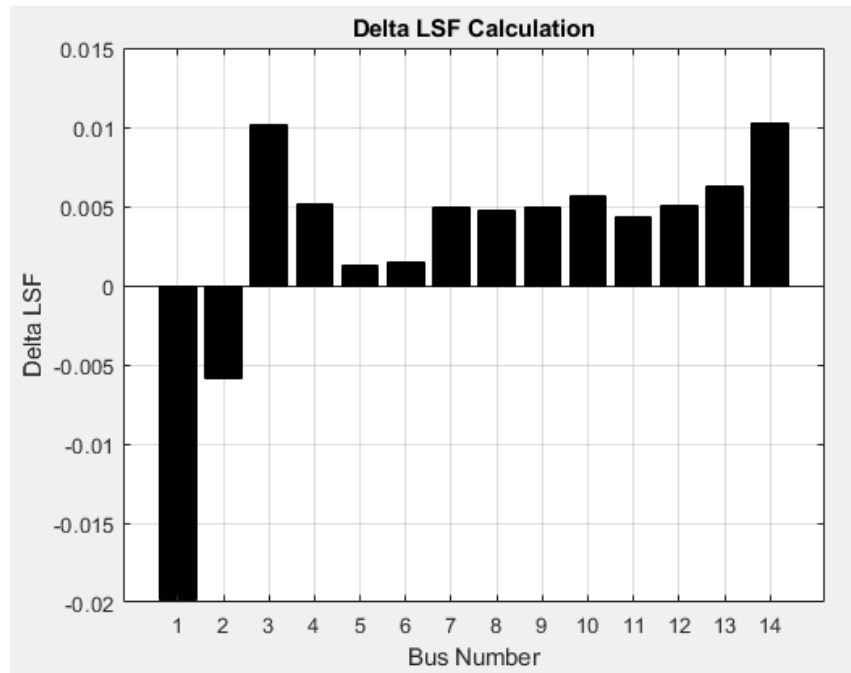


Figure 4.16. Δ LSF Calculation for 14-Bus Test Case

4.1.2.2 Test System-II: 9-Bus Case

Test System-II contains 9 buses. The total load demand of this system is 315.00 MW, and the same scaling procedure is applied according to hourly load demand as implemented for Test System-I.

Figure 4.17 and Figure 4.18 illustrate the daily LSF and Δ LSF calculations for Test System-II, respectively. When Δ LSF bar graph is analyzed, it is observed that Bus-7 points out itself, which shows the largest Δ LSF value by far. Note that, Δ LSF calculation for Bus-7 is 0.006688. For this reason, Bus-7 would be the bus to be selected for the BESS placement. According to the Δ LSF methodology, Figure 4.18 indicates that placing BESS to Bus-1 and Bus-3 would be the least practical procedure considering grid losses. Validation of locating BESS to the Bus-7 and the other buses will be examined by comparing grid losses.

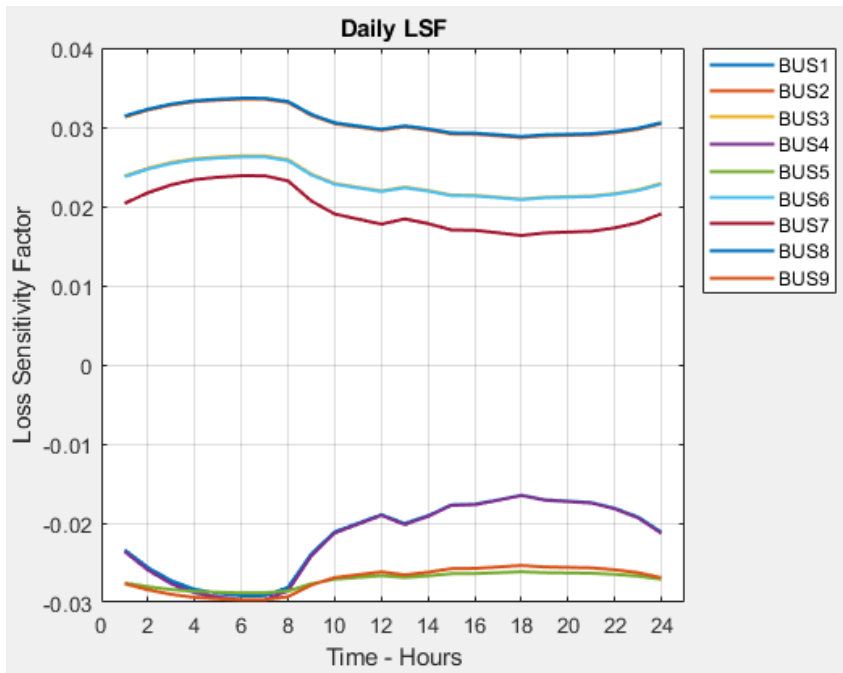


Figure 4.17. Daily LSF Calculation for 9-Bus Test Case

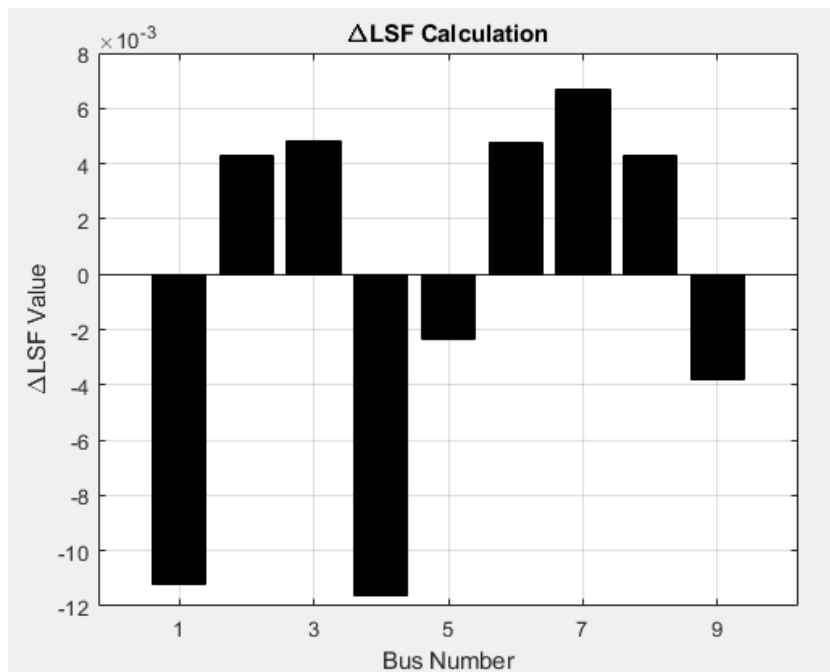


Figure 4.18. ΔLSF Calculation for 9-Bus Test Case

4.1.2.3 Test System-III: 33-Bus Case

Test System-III represents a distribution system, and unlike the other two test systems, the 33-bus grid structure is radial. Hence, this test system offers diversity to the method's evaluation. Before the hourly load demand scaling procedure, a power flow analysis is executed to the given 33-bus test case provided by IEEE, bus voltages are checked, and it is observed that the given load levels are satisfactory to take these load values as the maximum loads for buses.

Δ LSF calculation of Test System-III is given in Figure 4.19. The result indicates that locating the battery to Bus-6, Bus-7, or Bus-26 would give the optimum result considering to decrease in grid losses obtained from power flow studies. This argument will be validated afterwards by checking out grid losses. Also, there is another validation will be presented in the following section by comparing the Δ LSF method with the conventional LSF method.

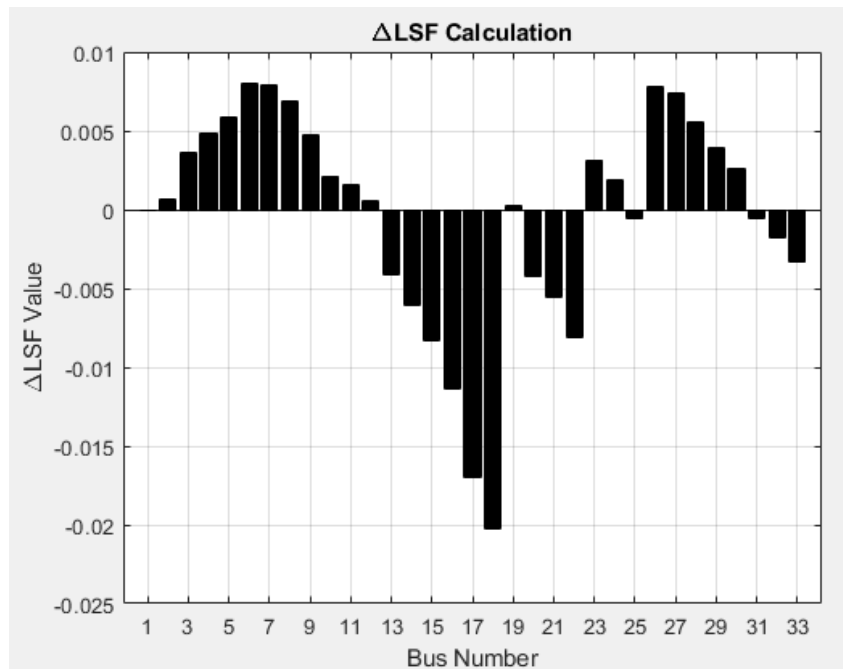


Figure 4.19. Δ LSF Calculation for 33-Bus Test Case

4.1.2.4 Validation of Δ LSF Method

Validation of Δ LSF method is discussed with three parts. In the first part, grid losses are calculated by implementing power flow analysis for each bus locations of BESS, and after that, loss values are compared each other to quantify the effect of BESS placement. In the second part, the conventional LSF method is calculated, and it is compared with the Δ LSF method, which is chosen as the optimum BESS placement method in this thesis. The third part verifies the LSF methodology by comparing losses found using power flow analysis and losses calculated from LSF values by multiplying LSF values with the increased injection at a bus due to BESS.

In the first validation part, it is aimed that placement of BESS to a bus where the location is found by applying the Δ LSF method should give the minimum grid losses result. Note that grid losses for the hours that the battery is in operation (6 hours) are given here for simplicity. Now, let us examine how much the system losses will be affected after locating BESS at the corresponding bus. Equation 3.1 and Equation 3.2 are used to observe the system losses. The hourly losses of the system with BESS are calculated with Equation 3.1 and Equation 3.2 based on the daily load curve given in Figure 4.14. The shaded areas given in Figure 4.14 are used for cases where BESS affects load and generation. In the first shaded area, BESS is in the charging state. Therefore, charging power at that hour is added to the total load of the system. On the other hand, the load is removed from the system since the BESS supports generation in the second shaded area. In this study, three different rated power of BESS (P^B) are assigned for loss calculation, 5 MW, 10 MW, and 15MW for Test System-I and II, 0.2 MW for Test System-III. Since charging and discharging duration are assigned as three hours, the BESS acts as a load with the given rated BESS power during these hours. However, the BESS cannot be discharged at the same power rate due to round-trip efficiency (RE). The rated output power during discharging is found by using Equation 4.1, which is derived from Equation 3.11.

$$P_{\text{rated,discharging}}^B = RE * P_{\text{rated,charging}}^B \quad (4.1)$$

As stated in Chapter 3, the RE is taken as 0.95. For instance, if the charging power of the battery is assumed as 10 MW, then the rated output power is 9.5 MW per hour for three hours during the discharging period, which is found by using Equation 4.1.

In Table 4.1, total grid losses calculation results are given for Test System-I. In this table, BESS location column shows the location of the battery, and grid losses are given for three P^B rates on the right side of the ΔLSF column. Grid losses are calculated during the operation of battery for corresponding BESS rated powers, and hence, losses are calculated for 6 hours. As it is concluded in ΔLSF method calculation section, Bus-3 or Bus-14 would be the optimum BESS location considering grid loss reduction. Table 4.1 shows that Bus-3 is an optimum option for BESS placement since grid losses are the least for all three P^B s. Note that grid losses without BESS are same as the grid losses obtained for Bus-1 for all three test systems since Bus-1 is slack bus, and variation of generation or load yield no effect.

Table 4.1. Grid Losses During Operation of BESS for Test System-I

BESS Location	ΔLSF	Grid Losses During Operation of BESS - MWh		
		$P^B = 5 \text{ MW}$	$P^B = 10 \text{ MW}$	$P^B = 15 \text{ MW}$
Bus-1	-0.01989	59.8970	59.8970	59.8970
Bus-2	-0.00584	59.7124	59.5761	59.4880
Bus-3	0.01016	59.5078	59.2742	59.1963
Bus-4	0.00512	59.5747	59.3462	59.2115
Bus-5	0.00129	59.6271	59.4377	59.3288
Bus-6	0.00151	59.6407	59.5034	59.4852
Bus-7	0.00495	59.5782	59.3630	59.2516
Bus-8	0.00477	59.5783	59.3637	59.2530
Bus-9	0.00498	59.5847	59.3904	59.3143
Bus-10	0.00566	59.6059	59.4928	59.5581
Bus-11	0.00432	59.6521	59.6346	59.8450
Bus-12	0.00508	59.7169	59.9113	60.4818
Bus-13	0.00629	59.6305	59.6023	59.8128
Bus-14	0.01029	59.6186	59.6786	60.0786

In Table 4.2, grid losses calculation results during the operation of battery are given for the 9-Bus Case, Test System-II. It is expected that Bus-7 should give minimum results as per calculated in Δ LSF method calculation section for Test System-II. The result indicates that locating BESS to Bus-7 would be an optimum selection. Test System-I and II have similar grid structure and load/generation profiles. To diversify the validation, Test System-III will be implemented.

Table 4.2. Grid Losses During Operation of BESS for Test System-II

BESS Location	Δ LSF	Grid Losses During Operation of BESS - MWh		
		$P^B = 5$ MW	$P^B = 10$ MW	$P^B = 15$ MW
Bus-1	-0.0112	30.3269	30.3269	30.3269
Bus-2	0.00423	30.0912	29.9328	29.8513
Bus-3	0.0048	30.0938	29.9449	29.8799
Bus-4	-0.0116	30.3266	30.3263	30.3261
Bus-5	-0.0024	30.2104	30.1356	30.1027
Bus-6	0.0048	30.0940	29.9446	29.8785
Bus-7	0.0067	30.0678	29.8901	29.7938
Bus-8	0.0043	30.0916	29.9320	29.8479
Bus-9	-0.0038	30.2225	30.1460	30.0972

As it is stated before, Test System-III is a radial distribution system that has 3.92 MW peak generation. Test System-III contains 33 buses, and it can be estimated that candidate buses for optimal BESS placement could be more than one. Note that, Δ LSF method determines that BESS should be placed to Bus-6, Bus-7, or Bus-26. Grid losses during the operation of battery are given in Table 4.3. This table confirms that locating battery to Bus-6, Bus-7, or Bus-26 results in the least losses. Also, it is concluded that locating BESS to Bus-7 would yield minimum grid losses.

Table 4.3 Grid Losses During Operation of BESS for Test System-III

BESS Location	Δ LSF	Grid Losses During Operation of BESS - MWh
		PB = 0.2 MW
Bus-1	-2 x 10 ⁻⁸	1.01463
Bus-2	0.00067	1.01425
Bus-3	0.00366	1.01251
Bus-4	0.00480	1.01174
Bus-5	0.00586	1.01101
Bus-6	0.00800	1.00949
Bus-7	0.00788	1.00946
Bus-8	0.00690	1.00963
Bus-9	0.00470	1.01029
Bus-10	0.00213	1.01114
Bus-11	0.00160	1.01133
Bus-12	0.00053	1.01171
Bus-13	-0.00414	1.01350
Bus-14	-0.00605	1.01426
Bus-15	-0.00833	1.01520
Bus-16	-0.01136	1.01645
Bus-17	-0.01698	1.01886
Bus-18	-0.02025	1.02025
Bus-19	0.00023	1.01441
Bus-20	-0.00425	1.01609
Bus-21	-0.00558	1.01660
Bus-22	-0.00807	1.01756
Bus-23	0.00316	1.01259
Bus-24	0.00187	1.01291
Bus-25	-0.00060	1.01381
Bus-26	0.00776	1.00952
Bus-27	0.00736	1.00960
Bus-28	0.00557	1.01006
Bus-29	0.00392	1.01055
Bus-30	0.00264	1.01099
Bus-31	-0.00058	1.01224
Bus-32	-0.00178	1.01274
Bus-33	-0.00335	1.01342

This validation indicates the positive effect of adding BESS to the test systems by checking out the total power losses. The system losses were reduced for all test systems. Now, the second validation part about comparison of conventional LSF and Δ LSF method will be discussed. For this comparison, Test System-III is used, and conventional LSF calculation is implemented based on peak load demand for the buses. The conventional LSF method suggests locating BESS to the bus with minimum LSF value for the peak load demand conditions. Figure 4.20 indicates that Bus-18 would be the optimum BESS location according to the conventional LSF methodology. However, Bus-18 is one of the deficient locations considering grid losses by checking out Table 4.3. Also, other buses that have lower LSF values, such as Bus-17, result in higher losses. This validation confirms that the conventional LSF method is not adequate for BESS applications since the method considers the battery is always in discharging mode.

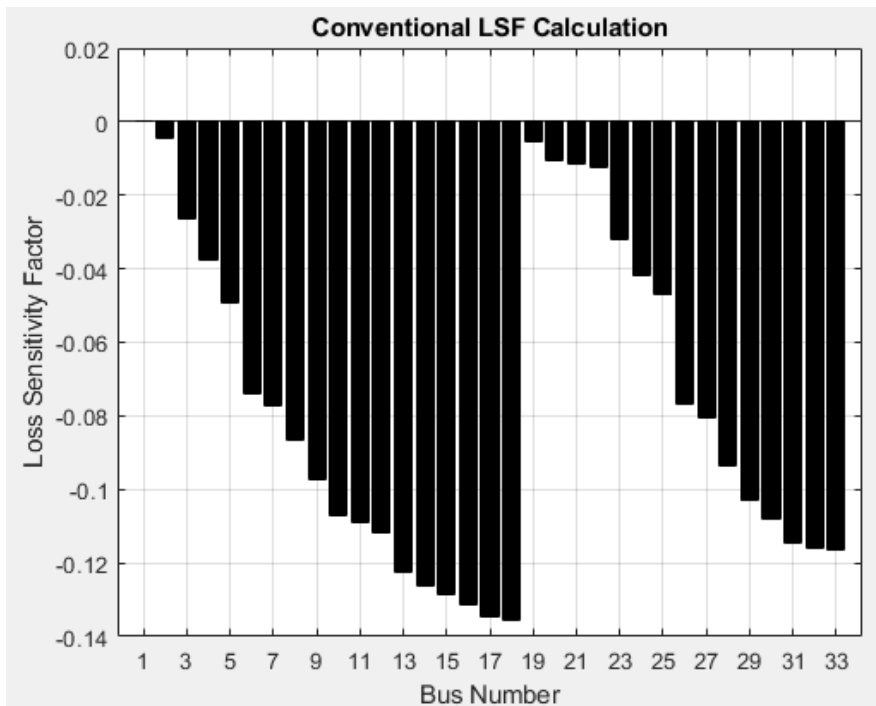


Figure 4.20. Conventional LSF Calculation for Test System-III

In the third part of the validation, the applicability of LSFs and hence the approach used in this study which is based on Δ LSF, will be verified. The variation of total system losses with respect to increased power injection at a certain bus has been investigated by two methods:

- i) By using the load flow analysis: The battery rating (i.e., as power injection to a specific bus) has been increased in steps and the changes in system loss have been determined.
- ii) By using the LSF computed at a certain bus: The LSF value computed has been multiplied by increments of different battery ratings.

Test System- II, 9-Bus test case, is used for loss variation comparison. For the comparison, the 9-Bus test system's load demand values are scaled to the levels that are obtained from the hourly load demand curve for a discharging hour, i.e., at 9 pm. As an example, two different busses (Bus-8 and Bus-9) have been selected. For the load flow case, the rating of the battery connected to one of these busses is increased in 1 MW increments from 1 MW to 10 MW, and the changes in system losses from no BESS case have been computed. Then, LSF values at these busses at 9 pm are computed. LSF value of Bus-8 is 0.02917, and this value is -0.02566 for Bus-9. Similarly, injected power levels (battery ratings) at these busses are changed from 1 MW to 10 MW with a 1 MW increment.

In theory, LSF indicates the amount of change in grid losses due to injected power variation at the relevant bus. Hence, grid losses variation can be approximately found by multiplying the LSF value at that bus with the rating of the battery connected at that bus. Figure 4.21 illustrates the variation in system losses obtained from two methods at Bus-8. Also, Figure 4.22 shows the loss variation comparison for Bus-9. The deviation between these two methods grows as the battery rating increases. These results demonstrate that loss variation calculated from LSF is comparably similar to the exact loss variation calculated by power flow analysis when the battery rating is small. It is observed that LSF based methods would give reliable results for relatively small injected power values.

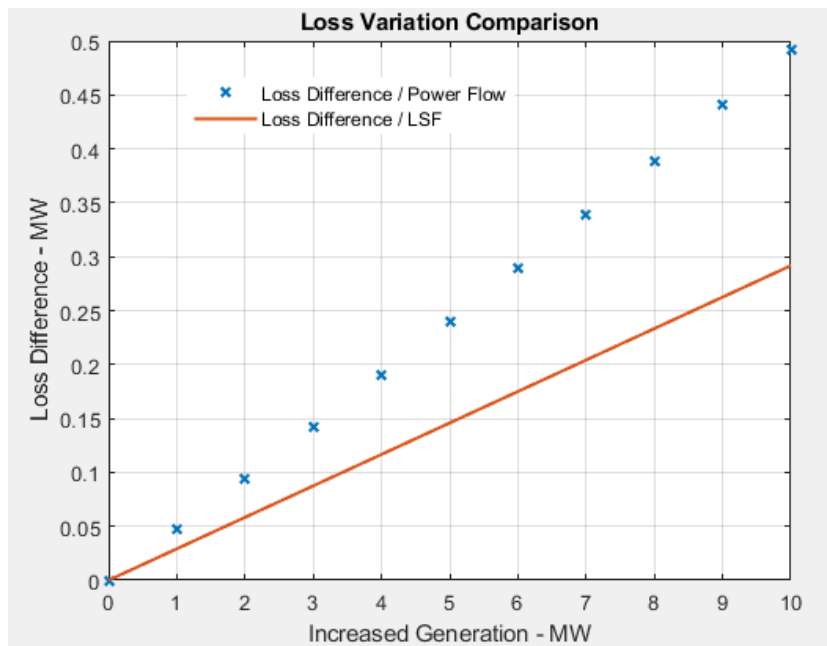


Figure 4.21. Variation of Losses with Increased Injection by Two Loss Calculation Methods at Bus-8

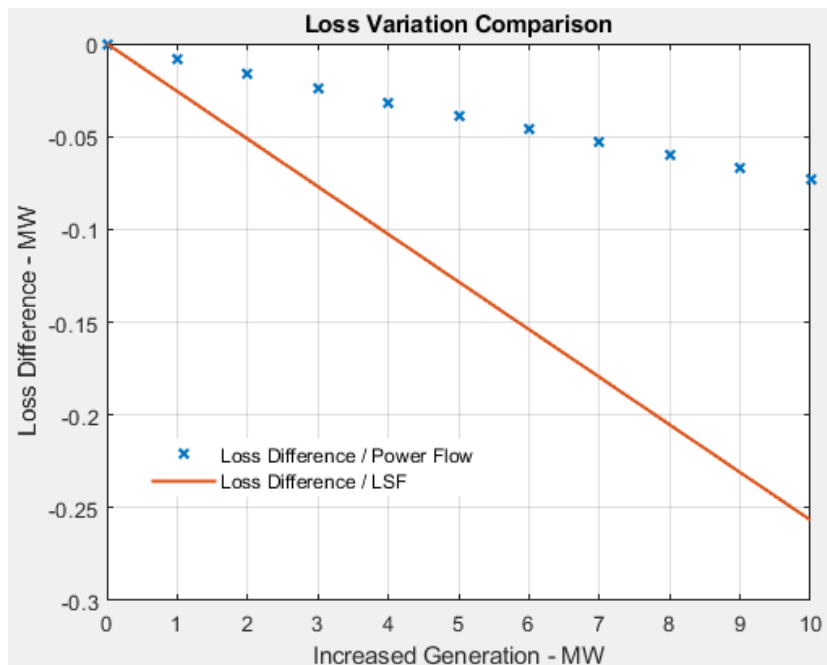


Figure 4.22. Variation of Losses with Increased Injection by Two Loss Calculation Methods at Bus-9

4.2 Evaluation of Cost-Benefit Analysis According to BESS Sizes

The main objective of the cost-benefit analysis is to determine a BESS size that returns its investment by using the savings obtained from electrical energy trading and reduced losses due to BESS. This study presents explanations to the readers if their BESS investment can pass the breakeven point during the floating life of the battery. Note that the breakeven point is the years at which savings coming from energy trading and reduced losses equals BESS investment expenses, and net income is zero. There are two different energy prices studies presented for the analysis. The first energy price curve (Daily Energy Price Curve-I) is obtained from EXIST, which is a synthetic curve. The second energy price curve (Daily Energy Price Curve-II) belongs to Illinois Institute of Technology Microgrid. These two energy markets demonstrate the significance of electrical energy prices, considering the purpose of getting the breakeven point before BESS's floating life is over by using savings obtained.

Equations 3.7, 3.8, 3.9, 3.10, and 3.11 will be used for the cost-benefit analysis. The analysis will be implemented for three different power ratings of BESS, i.e., 5 MW, 10 MW, and 15 MW. LRC will be obtained from the losses given in Table 4.1 since the highest loss reduction occurs in Test System-I, i.e., IEEE 14-Bus case. Similar analysis can be implemented for other loss reduction rates achieved for Test Systems II and III. Loss reduction rates that will be used for this analysis are given in Table 4.4. Note that given loss reduction rates calculated during a day, in other words, these losses values are calculated for 24-hours.

Table 4.4. Loss Reduction Rates Corresponds to P^B for Test System-I

Rated Power of BESS (P^B) - MW	Loss Reductions During 24-Hours – MWh	Reduced Loss During 3-Hours Discharging Mode – MWh	Increased Loss During 3-Hours Charging Mode – MWh
5	0.3188	1.5227	1.2039
10	0.5340	2.9950	2.4610
15	0.6454	4.4170	3.7716

For the Daily Energy Price Curve-I study, the obtained price curve in Figure 4.14 is used. Hence, the electrical energy market prices during the charging and discharging of BESS are taken as follows.

- Price at the time 6 am: 18.43 \$/MWh
- Price at the time 7 am: 17.85 \$/MWh
- Price at the time 8 am: 17.41 \$/MWh
- Price at the time 8 pm: 28.05 \$/MWh
- Price at the time 9 pm: 28.14 \$/MWh
- Price at the time 10 pm: 27.39 \$/MWh

Our charging/discharging strategy is assumed as one complete cycle per day. In this study, the BESS cycle number will be 3600 during the operation life since the floating life of Li-ion battery is 10 years, as given in Table 3.3. Note that DOD is taken as 90%, which satisfies cycle number stated in Table 3.3. The capacity of BESS is calculated by substituting P_{rated} in Equation 3.11.

Table 4.5 shows the LRC calculation results using Equation 3.10. In this calculation, loss reduction values given in Table 4.4 and energy prices indicated above are employed. LRC indicates the savings obtained from loss reduction due to the BESS usage.

Table 4.5. Savings Obtained from Loss Reduction Cost During the BESS’s Life for Test System-I and Daily Energy Price Curve-I

Rated Power of BESS (P^B) - MW	Cost Increase Due to Losses Occur During Charging - \$	Savings Obtained Due to Decreased Losses During Discharging - \$	Savings Obtained from Loss Reduction Cost - \$
5	77,564	152,721	75,175
10	158,557	300,386	141,829
15	242,997	443,007	200,010

In Table 4.6, the total savings coming from energy arbitrage and loss reduction are given by using the energy prices provided for Daily Energy Price Curve-I with the corresponding rated BESS power values. For this calculation, arbitrage cost is found and summed up with loss reduction cost to get the total savings obtained during the BESS's life. In Equation 3.7, this calculation is given in a detailed manner by explaining the components, and the result is named "Net Return".

Now, the storage system investment and operation costs will be calculated according to the BESS cost ratings that are given in Table 3.3. BESS investment cost is linearly proportional to its size, hence, there is no limitation with the increasing size of BESS except the investment budget and constructional limits. BESS cost calculation is performed according to the procedure described in Chapter 3.2. BESS cost ratings are given for the year 2022 in Table 3.3, and future cost ratings are calculated by using the reduction rates in Table 3.2. The results are given in

Table 4.7 for both the year 2022 and the year 2072. The result for the year 2072 is given because BESS investment and operation costs will be reduced enough to get the breakeven point for returning BESS expenses using the savings obtained from energy trading for Daily Energy Price Curve-I. Notice that the BESS investment and operation cost for 2072 is less than the total savings in 10 years during the storage system's life.

As conclusion, the study shows that it is not possible to obtain financial return from energy trading in 50 years with the assumed hourly prices for the test system used. If the cost reduction rate is assumed to be 5.5% per year, BESS investment considering only energy trading would be advantageous by the year 2072 for this energy market. Note that battery systems have many additional benefits besides utilizing variations of daily energy prices. However, in this thesis work, the energy trading application area is one and only consideration for the cost-benefit analysis. Following this study, Daily Energy Price Curve-II is chosen, which has a much greater difference between peak and off-peak periods of energy prices in a day.

Table 4.6. Total Savings Obtained from Energy Trading and Loss Reduction with Corresponding BESS Power Ratings for Daily Energy Price Curve-I

$P_{\text{rated}}^{\text{B}}$ charging /discharging MW	Charging Prices \$/MWh	Discharging Prices \$/MWh	Arbitrage Savings - \$	Total Savings in 10 Years Floating Life \$
5 / 4.75	18.43,	28.05, 28.14, 27.39	462,800	537,973
10 / 9.5	17.85,		925,600	1,067,425
15 / 14.25	17.41		1,388,400	1,588,400

Table 4.7. BESS Investment and Operation Cost for Corresponding Power and Capacity Ratings for Daily Energy Price Curve-I

BESS Ratings P^{B} - MW / E^{B} - MWh	BESS Investment and Operation Cost - \$	
	Year 2022	Year 2072
5 / 17.54	7,183,000	518,470
10 / 35.09	14,366,000	1,036,900
15 / 52.63	21,549,000	1,555,400

For the Daily Energy Price Curve-II study, the energy prices of the Illinois Institute of Technology Microgrid system, which also contains BESS, are taken and analyzed [41]. In Figure 4.23, the energy prices of the microgrid (Daily Energy Price Curve-II) system are given. As seen from the figure, the energy price rises to 157 \$/MWh during peak hours and decreases to 8 \$/MWh at night. Again, 130 \$/MWh price difference occurs when the 3-hours windows are considered during the day. Charging and discharging hours are given as shaded areas in Figure 4.23.

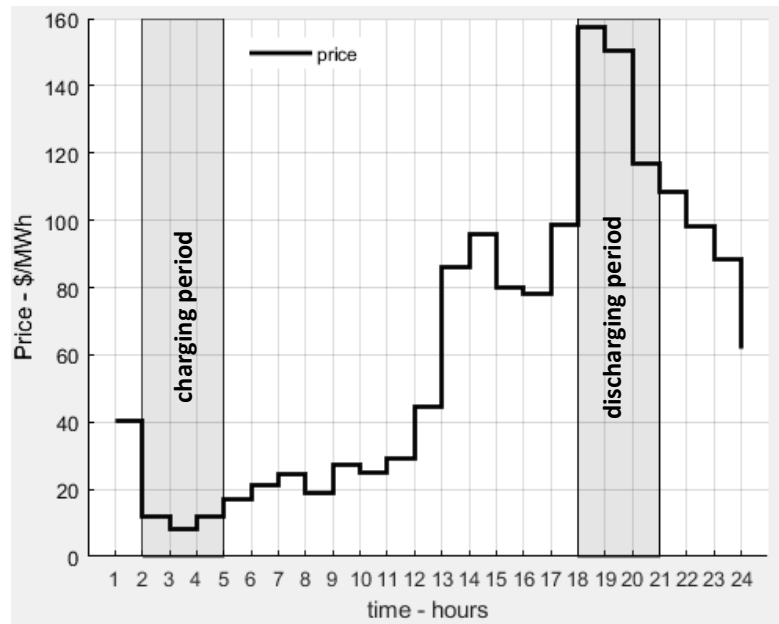


Figure 4.23. Electrical Energy Prices of Illinois Institute of Technology Microgrid

Table 4.8 shows the loss reduction savings resulting from energy trading according to Daily Energy Price Curve-II prices given in Figure 4.23. The difference in electrical energy prices seems to have a significant effect to get the breakeven point to return investment cost using energy trading. For the Daily Energy Price Curve-II case, financial savings are increased approximately ten times of the savings obtained in Daily Energy Price Curve-I.

Afterward, total savings obtained from energy trading and loss reduction are calculated. Table 4.9 indicates that constructing BESS into the Illinois Institute of Technology Microgrid System will become financially feasible in 2022, considering energy trading savings. Note that the BESS investment and operation cost for the year 2022 has already been calculated in Table 4.7.

Table 4.8. Savings Obtained from Loss Reduction Cost During the BESS's Life for Test System-I and Daily Energy Price Curve-II

Rated Power of BESS (P^B) - MW	Cost Increase Due to Losses Occur During Charging - \$	Savings Obtained Due to Decreased Losses During Discharging - \$	Savings Obtained from Loss Reduction Cost - \$
5	46,680	776,580	729,900
10	95,500	1,527,500	1,432,000
15	146,400	2,252,700	2,106,300

Table 4.9. Total Savings Obtained from Energy Trading and Loss Reduction with Corresponding BESS Power Ratings for Daily Energy Price Curve-II

P^B_{rated} charging /discharging MW	Charging Prices \$/MWh	Discharging Prices \$/MWh	Arbitrage Savings - \$	Total Savings in 10 Years Floating Life \$
5 / 4.75	12.00,	157.67,	6,685,500	7,415,000
10 / 9.5	8.00,	150.33,	13,371,000	14,803,000
15 / 14.25	12.00	117.00	20,056,500	22,163,000

The results given in Table 4.10 proves that the BESS investment can yield financial returns during its lifetime in an electrical energy market where large price variations in a day exist, i.e., Daily Energy Price Curve-II. Considering the given energy prices for Daily Energy Price Curve-II, the return time of investment is approximately 9.7 years for 5-10-15 MW battery ratings. Table 4.10 shows that the return time of the investment is almost the same for all the given power ratings in this study. It should be noted that the return time of the BESS investment would decrease by quantifying other application areas of the BESS in addition to energy trading and loss reduction, i.e., ancillary services, black start, supplemental reserve for vital areas.

Table 4.10 BESS Investment Cost and Total Savings Obtained from BESS
Operation for Daily Energy Price Curve-II

P_{rated}^B charging /discharging MW	BESS Capacity E^B - MWh	BESS Investment and Operation Cost in 2022 - \$	Total Savings in 10 Years Floating Life \$
5 / 4.75	17.54	7,183,000	7,415,000
10 / 9.5	35.09	14,366,000	14,803,000
15 / 14.25	52.63	21,549,000	22,163,000

4.3 Discussion on Testing and Evaluation

This chapter presents the results of the tests performed using the methodology proposed in Chapter 3. In the first step, the process of finding the optimal BESS placement location is tested and verified by load flow analysis on three different power grids, i.e., Test System-I, II, and III. The Δ LSF calculation is selected for optimal BESS placement method instead of the LSF calculation since LSF method considers only discharging mode of the battery and ignores charging mode. The drawback of the LSF method has been also presented by using Test System-III in the validation section. The Δ LSF method proposes an optimum bus for BESS placement to decrease the grid losses considering batteries act as a load during charging and supply the system when discharging. In the validation section, variation of grid losses after locating BESS to the system has been investigated. According to the validation done here, Δ LSF calculation is an accurate approach for the optimal placement of battery storage systems. However, it should not be forgotten that, the accuracy of LSF based methods are limited with small size of storage systems. This limitation has been investigated and presented in the validation section of optimal BESS placement topic.

In the second step, the relationship between BESS investments and battery size is examined. The calculation of the BESS investment cost amortization from electrical

energy trading is examined by taking advantage of the daily electrical energy price difference for two different time periods, i.e., Daily Energy Price Curve-I and II. According to the results, it is unfavorable to invest in a BESS application where the electrical energy market price difference is low (Daily Energy Price Curve-I) if the investor's objective is returning BESS expenses from energy trading during the floating life of the battery system. On the other hand, it has been shown that a positive net return can be achieved from the microgrid belonging to the Illinois Institute of Technology (Daily Energy Price Curve-II) by using BESS. It is because the electrical energy price difference in a day is larger in the given microgrid than Daily Energy Price Curve-I. Furthermore, various evaluations are shown by taking into account the annual price decrease in BESS installation prices due to technological developments.

CHAPTER 5

CONCLUSION AND FUTURE WORKS

Since the battery technologies have reached to a level that batteries can provide great power and current today brings the idea of using them in power system applications. Batteries basically have the ability to store energy, keep it for a certain period of time, and transfer that energy to the grid when needed in a power system. Battery energy storage systems are also preferred because the conversion losses are pretty low.

Acting as a load or supporting generation abilities of BESS become more problematic when high-level power ratings are considered. Incorrect positioning of battery systems can cause excessive system losses, voltage spikes and unstable conditions in the network. The main motivation of this thesis work is to propose optimal placement of battery storage systems and sizing of it considering financial concerns.

To determine the BESS location, an approach based on loss sensitivity factor (LSF) is proposed. The LSF calculation method estimates how much the system losses will be affected by variation in generation or load in a bus by one unit. In this thesis, a method based on LSF calculation is applied by considering the charging/discharging modes, which are the two operation modes where the battery acts as both load and generation. The method that considers both charging and discharging modes of the battery is known as Δ LSF method, where as conventional LSF approach assumes that battery operates in only discharging mode. In the scope of this work, the optimal placement calculations are evaluated for three different test systems, i.e., 14-Bus, 9-Bus, and 33-Bus test cases.

The other main focus of this study is the cost-benefit analysis of BESS investment. Various cost parameters are used in the analysis, such as capacity rating, power

rating, operation and maintenance, construction, balance of plant. These parameters generally depend on the battery system's rated output power and capacity. Battery aging caused by charging/discharging cycles is also taken into account by using the term depth of discharge. Decreasing trend on battery system investment costs are considered and plans for the following years are put forward. In the cost-benefit analysis, the BESS results in savings by making electrical energy trading. Reduction of system losses due to BESS operation is also taken into account for the savings calculation. In this study, calculations are performed to determine the breakeven point, which indicates that the BESS investment expenses are equal to savings obtained from BESS operation. Two energy markets are chosen for the cost-benefit analysis to point out the importance of the energy price differences within a day. This study shows that it is not feasible to return the battery's investment and operation costs in an electrical energy market where small price variations in a day exist. However, it is also shown that this investment will be beneficial in a system that has large electrical energy price differences within a day. A real microgrid system in the USA is used to present a convincing case for BESS investment where the electrical energy price differences are high. It should be noted that feasibility of BESS investment depends on a given daily load curve, power system configuration, and energy market prices.

Battery systems are preferred in various power system services such as ancillary services, black start, congestion management, loss reduction, emergency supply for vital areas, and electricity balancing market. In further studies, even if the investment of a battery system seems to be disadvantageous when the objective is getting financial savings from energy trading in a specific energy market, a cost-benefit analysis can be performed by quantifying other application areas of the BESS in addition to energy trading.

REFERENCES

- [1] Zhang, Yongxi & Ren, Shuyun & Dong, Z.Y. & Xu, Yan & Zheng, Yu. (2017). Optimal Placement of Battery Energy Storage in Distribution Networks Considering Conservation Voltage Reduction and Stochastic Load Composition. *IET Generation, Transmission & Distribution*. 11. 10.1049/iet-gtd.2017.0508.
- [2] L. Vankudoth and A. Q. H. Badar, "Distribution Network Optimization through Siting and Sizing of BESS," 2019 8th International Conference on Power Systems (ICPS), 2019, pp. 1-5, doi: 10.1109/ICPS48983.2019.9067342.
- [3] S. Salee and P. Wirasanti, "Optimal Siting and Sizing of Battery Energy Storage Systems for Grid-Supporting in Electrical Distribution Network," 2018 International ECTI Northern Section Conference on Electrical, Electronics, Computer and Telecommunications Engineering (ECTI-NCON), 2018, pp. 100-105, doi: 10.1109/ECTI-NCON.2018.8378290.
- [4] F. García-Muñoz, F. Díaz-Gonzalez, C. Corchero and C. Nuñez-de-Toro, "Optimal Sizing and Location of Distributed Generation and Battery Energy Storage System," 2019 IEEE PES Innovative Smart Grid Technologies Europe (ISGT-Europe), 2019, pp. 1-5, doi: 10.1109/ISGTEurope.2019.8905609.
- [5] C. Essayeh, M. R. El-Fenni and H. Dahmouni, "Optimal Sizing of A PV-ESS Microgrid System Under Dynamic Pricing of Utility Energy," 2018 19th IEEE Mediterranean Electrotechnical Conference (MELECON), 2018, pp. 86-91, doi: 10.1109/MELCON.2018.8379073.
- [6] E. Zarezadeh, H. Fakharzadegan, A. Ghorbani and H. Fathabadi, "A Probabilistic Approach to Determine PV Array Size and Battery Capacity Used in Grid-Connected PV Systems," 2015 23rd Iranian Conference on Electrical Engineering, 2015, pp. 1533-1538, doi: 10.1109/IranianCEE.2015.7146463.

- [7] V. Sharma, M. H. Haque and S. M. Aziz, "Optimal Battery Size for Grid Connected Rooftop Solar Photovoltaic Systems in South Australia," 2017 Australasian Universities Power Engineering Conference (AUPEC), 2017, pp. 1-6, doi: 10.1109/AUPEC.2017.8282509.
- [8] Xiao, J., Zhang, Z., Bai, L. and Liang, H. (2016), "Determination of The Optimal Installation Site and Capacity of Battery Energy Storage System in Distribution Network Integrated with Distributed Generation," IET Gener. Transm. Distrib., 10: 601-607.
- [9] H. Pandžić, Y. Wang, T. Qiu, Y. Dvorkin and D. S. Kirschen, "Near-Optimal Method for Siting and Sizing of Distributed Storage in a Transmission Network," in IEEE Transactions on Power Systems, vol. 30, no. 5, pp. 2288-2300, Sept. 2015, doi: 10.1109/TPWRS.2014.2364257.
- [10] S. Shafiq, B. Khan and A. T. Al-Awami, "Optimal Battery Placement in Distribution Network Using Voltage Sensitivity Approach," 2019 IEEE Power and Energy Conference at Illinois (PECI), 2019, pp. 1-4, doi: 10.1109/PECI.2019.8698781.
- [11] S. Sundhararajan and A. Pahwa, "Optimal Selection of Capacitors for Radial Distribution Systems Using a Genetic Algorithm," in IEEE Transactions on Power Systems, vol. 9, no. 3, pp. 1499-1507, Aug. 1994, doi: 10.1109/59.336111.
- [12] K. Prakash and M. Sydulu, "Particle Swarm Optimization Based Capacitor Placement on Radial Distribution Systems," 2007 IEEE Power Engineering Society General Meeting, 2007, pp. 1-5, doi: 10.1109/PES.2007.386149.
- [13] P. Kumar, A. K. Singh and N. Singh, "Sensitivity Based Capacitor Placement: A Comparative Study," 2011 6th International Conference on Industrial and Information Systems, 2011, pp. 381-385, doi: 10.1109/ICIINFS.2011.6038098.

- [14] S. Paul and W. Jewell, "Optimal Capacitor Placement and Sizes for Power Loss Reduction Using Combined Power Loss Index-Loss Sensitivity Factor and Genetic Algorithm," 2012 IEEE Power and Energy Society General Meeting, 2012, pp. 1-8, doi: 10.1109/PESGM.2012.6345635.
- [15] S. B. Karanki, D. Xu, B. Venkatesh and B. N. Singh, "Optimal Location of Battery Energy Storage Systems in Power Distribution Network for Integrating Renewable Energy Sources," 2013 IEEE Energy Conversion Congress and Exposition, 2013, pp. 4553-4558, doi: 10.1109/ECCE.2013.6647310.
- [16] T. K. A. Brekken, A. Yokochi, A. von Jouanne, Z. Z. Yen, H. M. Hapke and D. A. Halamay, "Optimal Energy Storage Sizing and Control for Wind Power Applications," in IEEE Transactions on Sustainable Energy, vol. 2, no. 1, pp. 69-77, Jan. 2011, doi: 10.1109/TSTE.2010.2066294.
- [17] C. D. Widjaja, F. S. Rahman, K. M. Banjar-Nahor and N. Hariyanto, "A Novel Approach of Loss Sensitivity Factor for Optimal Placement of Battery Energy Storage System," 2021 22nd IEEE International Conference on Industrial Technology (ICIT), 2021, pp. 535-540, doi: 10.1109/ICIT46573.2021.9453579.
- [18] J. Sardi, N. Mithulananthan and D. Q. Hung, "A Loss Sensitivity Factor Method for Locating ES in a Distribution System with PV Units," 2015 IEEE PES Asia-Pacific Power and Energy Engineering Conference (APPEEC), 2015, pp. 1-5, doi: 10.1109/APPEEC.2015.7380873.
- [19] J. Eyer and G. Corey, "Energy Storage for The Electricity Grid: Benefits and Market Potential Assessment Guide; A Study for The DoE Energy Storage Systems Program," Sandia Nat. Lab., Albuquerque, NM, USA, Sandia Rep. SAND2010-0815, 2010.
- [20] Amini, M., Khorsandi, A., Vahidi, B., Hosseinian, S. H., & Malakmahmoudi, A. (2021). Optimal Sizing of Battery Energy Storage in A Microgrid Considering Capacity Degradation and Replacement Year. Electric Power Systems Research, 195, 107170.

[21] I. Alsaïdan, A. Khodaei and W. Gao, "A Comprehensive Battery Energy Storage Optimal Sizing Model for Microgrid Applications," in *IEEE Transactions on Power Systems*, vol. 33, no. 4, pp. 3968-3980, July 2018, doi: 10.1109/TPWRS.2017.2769639.

[22] Wikimedia Commons [Online], Available:

https://commons.wikimedia.org/wiki/File:Electricity_Grid_Schematic_English.svg

[23] Energy Exchange Istanbul [Online], Available:

<https://seffaflik.epias.com.tr/transparency/>

[24] M. Emmanuel, A. Jain, R. Bryce, A. Latif, S. Ghosh and A. Nagarajan, "Impacts of Control Set-Points on Battery Energy Storage Performance for Peak Shaving Application," 2020 47th IEEE Photovoltaic Specialists Conference (PVSC), 2020, pp. 2703-2707, doi: 10.1109/PVSC45281.2020.9301022.

[25] Schumm, Brooke. "Battery". *Encyclopedia Britannica*, 5 Mar. 2021, <https://www.britannica.com/technology/battery-electronics>. Accessed 22 December 2021.

[26] N. Meena et al., "Charging and Discharging Characteristics of Lead acid and Li-ion batteries," 2014 Power and Energy Systems: Towards Sustainable Energy, 2014, pp. 1-3, doi: 10.1109/pestse.2014.6805253.

[27] Daiwon Choi, Nimat Shamim, Alasdair Crawford, Qian Huang, Charlie K. Vartanian, Vilayanur V. Viswanathan, Matthew D. Paiss, Md Jan E. Alam, David M. Reed, Vince L. Sprenkle, "Li-ion Battery Technology for Grid Application," *Journal of Power Sources*, Volume 511, 2021, 230419, ISSN 0378-7753,

[28] K. Wongwut and S. Nuchprayoon, "Optimum Hourly Operation of a Prosumer with Battery Energy Storage System Under Time-of-Use Pricing," 2017 IEEE PES Asia-Pacific Power and Energy Engineering Conference (APPEEC), 2017, pp. 1-6, doi: 10.1109/APPEEC.2017.8308997.

- [29] A. Mohsenian-Rad and A. Leon-Garcia, "Optimal Residential Load Control with Price Prediction in Real-Time Electricity Pricing Environments," in *IEEE Transactions on Smart Grid*, vol. 1, no. 2, pp. 120-133, Sept. 2010, doi: 10.1109/TSG.2010.2055903.
- [30] Fossati, Juan & Galarza, Ainhoa & Martín-Villate, Ander & Fontan, L.. (2015), "A Method for Optimal Sizing Energy Storage Systems for Microgrids," *Renewable Energy*, 77. 539-549. 10.1016/j.renene.2014.12.039.
- [31] J. A. P. Lopes, C. L. Moreira and A. G. Madureira, "Defining Control Strategies for Microgrids Islanded Operation," In *IEEE Transactions on Power Systems*, vol. 21, no. 2, pp. 916-924, May 2006, doi: 10.1109/TPWRS.2006.873018.
- [32] P. Kundur, N. Balu and M. Lauby, *Power System Stability and Control*, New York: McGraw-Hill, 2009.
- [33] C. D. Aluthge, K. T. M. Udayanga Hemapala and J. R. Lucas, "Battery Energy Storage System to Improve Reliability due to Under Frequency Load Shedding," 2020 IEEE 5th International Conference on Computing Communication and Automation (ICCCA), 2020, pp. 571-576, doi: 10.1109/ICCCA49541.2020.9250889.
- [34] Grid-Scale Battery Storage [Online], Available: <https://www.nrel.gov/docs/fy19osti/74426.pdf>
- [35] Bergen, A. and Vittal, V., 2000. *Power Systems Analysis*. 2nd ed. Upper Saddle River, New Jersey: Prentice Hall.
- [36] Grainger, J., Stevenson, W. and Chang, G., 1994. *Power System Analysis*. Singapore: McGraw-Hill.
- [37] Elgerd, O., 1971. *Electric Energy Systems Theory: An Introduction*. New York: McGraw-Hill.

- [38] IEEE 14-Bus Power System Test Case [Online], Available: https://web.archive.org/web/20210506155359/http://labs.ece.uw.edu/pstca/pf14/pg_tca14bus.htm
- [39] Sieber, N. (1984). Chow, J. H. (ed.), Time-Scale Modeling of Dynamic Networks with Applications to Power Systems. Berlin-Heidelberg-New York, Springer-Verlag 1982 (Lecture Notes in Control and Information Sciences 46).
- [40] M. E. Baran and F. F. Wu, "Network Reconfiguration in Distribution Systems for Loss Reduction and Load Balancing," in IEEE Transactions on Power Delivery, vol. 4, no. 2, pp. 1401-1407, April 1989, doi: 10.1109/61.25627.
- [41] Illinois Institute of Technology Microgrid System [Online], Available: <http://iitmicrogrid.net/microgrid.aspx>
- [42] R. D. Zimmerman, C. E. Murillo-Sánchez and R. J. Thomas, "MATPOWER: Steady-State Operations, Planning, and Analysis Tools for Power Systems Research and Education," in IEEE Transactions on Power Systems, vol. 26, no. 1, pp. 12-19, Feb. 2011, doi: 10.1109/TPWRS.2010.2051168.
- [43] MATLAB. (May 5, 2020). 9.8.0.1380330 (R2020a). Natick, Massachusetts: The MathWorks Inc.

APPENDICES

A. IEEE 14-Bus Test Case Data

The IEEE 14-Bus test system characterizes the US Power System released in 1962. In the following tables, test case parameters are provided. Data are given in per unit case with 100 MVA base power.

Table A.1. IEEE 14-Bus System Bus Data

Bus No	Type	P _{demand} MW	Q _{demand} MVar	V _{max}	V _{min}
1	3	0	0	1.06	0.94
2	2	21.7	12.7	1.06	0.94
3	2	94.2	19	1.06	0.94
4	1	47.8	-3.9	1.06	0.94
5	1	7.6	1.6	1.06	0.94
6	2	11.2	7.5	1.06	0.94
7	1	0	0	1.06	0.94
8	2	0	0	1.06	0.94
9	1	29.5	16.6	1.06	0.94
10	1	9	5.8	1.06	0.94
11	1	3.5	1.8	1.06	0.94
12	1	6.1	1.6	1.06	0.94
13	1	13.5	5.8	1.06	0.94
14	1	14.9	5	1.06	0.94

Table A.2. IEEE 14-Bus System Generator Data

Bus No	P _{generation} MW	Q _{generation} MVar	Q _{max} MVar	Q _{min} MVar	V _g	P _{max} MW	P _{min} MW
1	232.4	-16.9	10	0	1.06	332.4	0
2	40	42.4	50	-40	1.045	140	0
3	0	23.4	40	0	1.01	100	0
6	0	12.2	24	-6	1.07	100	0
8	0	17.4	24	-6	1.09	100	0

Table A.3. IEEE 14-Bus System Branch Data

From Bus	To Bus	r	x	b
1	2	0.01938	0.05917	0.0528
1	5	0.05403	0.22304	0.0492
2	3	0.04699	0.19797	0.0438
2	4	0.05811	0.17632	0.034
2	5	0.05695	0.17388	0.0346
3	4	0.06701	0.17103	0.0128
4	5	0.01335	0.04211	0
4	7	0	0.20912	0
4	9	0	0.55618	0
5	6	0	0.25202	0
6	11	0.09498	0.1989	0
6	12	0.12291	0.25581	0
6	13	0.06615	0.13027	0
7	8	0	0.17615	0
7	9	0	0.11001	0
9	10	0.03181	0.0845	0
9	14	0.12711	0.27038	0
10	11	0.08205	0.19207	0
12	13	0.22092	0.19988	0
13	14	0.17093	0.34802	0

Voltages (V), branch resistance (r), branch reactance (x), and total line charging susceptance (b) are given as per unit.

B. 9-Bus Test System Data

This test system is extracted from [39]. In the following tables, test case parameters are provided. Data are given in per unit case with 100 MVA base power. Voltages (V), branch resistance (r), branch reactance (x), and total line charging susceptance (b) are given as per unit.

Table B.4. 9-Bus System Bus Data

Bus No	Type	P _{demand} MW	Q _{demand} MVar	Base kV	V _{max}	V _{min}
1	3	0	0	345	1.1	0.9
2	2	0	0	345	1.1	0.9
3	2	0	0	345	1.1	0.9
4	1	0	0	345	1.1	0.9
5	1	90	30	345	1.1	0.9
6	1	0	0	345	1.1	0.9
7	1	100	35	345	1.1	0.9
8	1	0	0	345	1.1	0.9
9	1	125	50	345	1.1	0.9

Table B.5. 9-Bus System Generator Data

Bus No	P _{generation} MW	Q _{generation} MVar	Q _{max} MVar	Q _{min} MVar	V _g	P _{max} MW	P _{min} MW
1	72.3	27.03	300	-300	1.04	250	10
2	163	6.54	300	-300	1.025	300	10
3	85	-10.95	300	-300	1.025	270	10

Table B.6. 9-Bus System Branch Data

From Bus	To Bus	r	x	b
1	4	0	0.0576	0
4	5	0.017	0.092	0.158
5	6	0.039	0.17	0.358
3	6	0	0.0586	0
6	7	0.0119	0.1008	0.209
7	8	0.0085	0.072	0.149
8	2	0	0.0625	0
8	9	0.032	0.161	0.306
9	4	0.01	0.085	0.176

C. IEEE 33-Bus Test System Data

The IEEE 33-Bus radial distribution test system parameters are given in the following tables. Data are given in per unit case with 10 MVA base power. Voltages (V), branch resistance (r), and branch reactance (x) are given as per unit. Status column in Table C.9 shows operation of the line, i.e., '0' -> disconnected from grid.

Table C.7. IEEE 33-Bus System Bus Data

Bus No	Type	P _{demand} MW	Q _{demand} MVar	Bs	Base kV	V _{max}	V _{min}
1	3	0.01	0.006	0.001	12.66	1	1
2	1	0.009	0.004	0	12.66	1.1	0.9
3	1	0.012	0.008	0	12.66	1.1	0.9
4	1	0.006	0.003	0	12.66	1.1	0.9
5	1	0.006	0.002	0	12.66	1.1	0.9
6	1	0.02	0.01	0	12.66	1.1	0.9
7	1	0.02	0.01	0	12.66	1.1	0.9
8	1	0.006	0.002	0	12.66	1.1	0.9
9	1	0.006	0.002	0	12.66	1.1	0.9
10	1	0.0045	0.003	0	12.66	1.1	0.9
11	1	0.006	0.0035	0	12.66	1.1	0.9
12	1	0.006	0.0035	0	12.66	1.1	0.9
13	1	0.012	0.008	0	12.66	1.1	0.9
14	1	0.006	0.001	0	12.66	1.1	0.9
15	1	0.006	0.002	0	12.66	1.1	0.9
16	1	0.006	0.002	0	12.66	1.1	0.9
17	1	0.009	0.004	0	12.66	1.1	0.9
18	1	0.009	0.004	0	12.66	1.1	0.9
19	1	0.009	0.004	0	12.66	1.1	0.9
20	1	0.009	0.004	0	12.66	1.1	0.9
21	1	0.009	0.004	0	12.66	1.1	0.9
22	1	0.009	0.005	0	12.66	1.1	0.9
23	1	0.042	0.02	0	12.66	1.1	0.9
24	1	0.042	0.02	0	12.66	1.1	0.9
25	1	0.006	0.0025	0	12.66	1.1	0.9
26	1	0.006	0.0025	0	12.66	1.1	0.9
27	1	0.006	0.002	0	12.66	1.1	0.9
28	1	0.012	0.007	0	12.66	1.1	0.9
29	1	0.02	0.06	0	12.66	1.1	0.9
30	1	0.015	0.007	0	12.66	1.1	0.9
31	1	0.021	0.01	0	12.66	1.1	0.9
32	1	0.006	0.004	0	12.66	1.1	0.9
33	1	0	0	0	12.66	1.1	0.9

Table C.8. IEEE 33-Bus System Generator Data

Bus No	P _{generation} MW	Q _{generation} MVA _r	Q _{max} MVA _r	Q _{min} MVA _r	V _g	P _{max} MW	P _{min} MW
1	0	0	10	-10	1	10	0

Table C.9. IEEE 33-Bus System Branch Data

From Bus	To Bus	r	x	b	Status
1	2	0.005752	0.002932	0	1
2	3	0.030759	0.015666	0	1
3	4	0.022835	0.011629	0	1
4	5	0.023777	0.012110	0	1
5	6	0.051099	0.044111	0	1
6	7	0.011679	0.038608	0	1
7	8	0.044386	0.014668	0	1
8	9	0.064264	0.046170	0	1
9	10	0.065137	0.046170	0	1
10	11	0.012266	0.004055	0	1
11	12	0.023359	0.007724	0	1
12	13	0.091592	0.072063	0	1
13	14	0.033791	0.044479	0	1
14	15	0.036873	0.032818	0	1
15	16	0.046563	0.034003	0	1
16	17	0.080423	0.107377	0	1
17	18	0.045671	0.035813	0	1
2	19	0.010232	0.009764	0	1
19	20	0.093850	0.084566	0	1
20	21	0.025549	0.029848	0	1
21	22	0.044230	0.058480	0	1
3	23	0.028151	0.019235	0	1
23	24	0.056028	0.044242	0	1
24	25	0.055903	0.043743	0	1
6	26	0.012665	0.006451	0	1
26	27	0.017731	0.009028	0	1
27	28	0.066073	0.058255	0	1
28	29	0.050176	0.043712	0	1
29	30	0.031664	0.016128	0	1
30	31	0.060795	0.060084	0	1
31	32	0.019372	0.022579	0	1
32	33	0.021275	0.033080	0	1
21	8	0.124785	0.124785	0	0
9	15	0.124785	0.124785	0	0
12	22	0.124785	0.124785	0	0
18	33	0.031196	0.031196	0	0
25	29	0.031196	0.031196	0	0